

J. VANIER 

Atomic clocks based on coherent population trapping: a review

Département de Physique, Université de Montréal, Montréal, QC, H3C 3J7, Canada; Kernco Inc.,
28 Harbor Street, Danvers, MA 01923-0678, USA

Received: 8 March 2005 / Revised version: 22 May 2005
Published online: 22 July 2005 • © Springer-Verlag 2005

ABSTRACT The paper gives an overview of the use of the coherent population trapping phenomenon (CPT) in alkali-metal atoms in the implementation of atomic frequency standards. Several avenues are examined. These include: the approach using a combination of the CPT phenomenon and the Ramsey separated interaction field technique on an atomic beam; the passive approach in a cell in which the microwave hyperfine resonance excited by the CPT phenomenon is detected directly on the transmitted radiation; the maser approach in which the same resonance is observed by means of stimulated emission in a microwave cavity-cell arrangement; and, finally, the proposed approach using pulses in a time sequence that implements the combined CPT–Ramsey separated interaction field technique in time rather than in space. A review of field and laboratory implementations using these approaches is made.

PACS 32.10.Fn; 32.30.Bv; 32.70.Jz; 32.80.Wr

1 Introduction

The last fifty years have been a period of outstanding developments in the field of atomic frequency standards [1]. This development has progressed by quantum leaps in the quality of the implementations to reach, at the present day, frequency stabilities in the 10^{-16} range in hydrogen masers [2, 3] and accuracies better than 1×10^{-15} in cesium fountains [4–7]. On the other hand, demand of standards for field use has led to the development by several industries of small units such as the field Cs beam clock and the optically pumped Rb frequency standard, for which frequency stability and size are of prime interest.

In all those classical implementations, the frequency of the transition between the two ground-state hyperfine levels of the atomic species chosen (hydrogen or an alkali-metal atom) serves as the atomic resonance frequency reference. This resonance, which is in the microwave range, is detected in all cases by means of the classical magnetic resonance technique [8]. Another common characteristic of those implementations is the use of state selection, by means of either


magnetic spatial deflection [9] or optical pumping [10], in the preparation of the atomic ensemble, a process that is required to enhance the detected resonance signal.

Coherent population trapping (CPT), accomplished by means of two laser radiation fields applied in a so-called Λ scheme [11], provides an alternative to these classical approaches. CPT makes possible preparation of the atomic ensemble and resonant excitation at the same time and same region of space. In the case of alkali atoms, the fields are applied to an ensemble of atoms in resonance with the transitions between the two hyperfine levels of the $S_{1/2}$ ground state and one of the P-state hyperfine levels, forming the Λ scheme. Due to inherent physical quantum properties, interference appears in the excitation process, coherence is created in the ground state, and the ensemble is placed in a non-absorbing state called a ‘dark state’. The phenomenon, as observed at a hyperfine frequency, was reported for the first time by Alzetta et al. in sodium by means of a multimode dye laser [11]. A related phenomenon was also reported by Bell and Bloom at the Zeeman frequency of Cs and Rb vapors using an amplitude-modulated spectral lamp [12].

The phenomenon may be observed in several ways. Since in CPT no atoms are excited to the P state at exact resonance, a narrow ‘black’ line in the fluorescence spectrum of the optically pumped ensemble is observed. Furthermore, since the system does not absorb energy at resonance, it becomes transparent. Consequently, the phenomenon can be observed either on the fluorescence as a black line (generally called a dark line) or on the transmitted radiation as an increase in transmission at resonance (often called a bright line). On the other hand, the ensemble is placed in a superposition state of the two alkali atom hyperfine ground state and coherence at the hyperfine frequency is created. This coherence, in turn, creates an oscillating magnetization that can be detected directly through stimulated emission in a cavity.

Early proposals were made on the use of the phenomenon in several applications such as magnetometry [13, 14], induced transparency [15–17], atom cooling [18], and precision spectroscopy [19], and its properties were studied in connection with state-selection improvement in optical pumping [20, 21].

On the other hand, the resonance phenomenon reflects all the properties of the hyperfine resonance in the ground state of the alkali atoms and may be used to implement an atomic frequency standard in the same way as is done in the classical

 E-mail: jac.vanier@sympatico.ca

approach using double-resonance microwave–optical pumping [21]. A first effort on the use of the phenomenon towards such a realization was reported by Thomas et al. [22]. In those experiments, the phenomenon was used on a sodium beam to implement a Ramsey type of separated interaction regions [23] entirely with light beams without the classical Ramsey microwave cavity. Serious efforts were also started in the mid 1990s on the application of the CPT phenomenon towards the use of sealed-off cells to implement small-scale atomic frequency standards [24–26]. The last effort [26] has led to the industrial implementation of a small, completely autonomous, passive frequency standard using ^{87}Rb [27, 28] as well as a laboratory-type CPT maser [29–31]. The phenomenon is also being studied with the goal of implementing an atomic clock based on CPT, using a laser-cooled atomic ensemble [32]. Finally, the phenomenon was also proposed in the implementation of a laboratory prototype of a so-called chip-scale optical package [33–36].

It is possible to interpret the phenomenon and most of the observations by means of a simple three-level model. In the case of atomic beams, the problem is simplified due to the free evolution of the atoms in the beam and the absence of relaxation. In the case of cells, with the presence of relaxation, the rate equations for the evolution of the energy-level populations and of the coherence created by the laser radiation fields in the ensemble may be solved exactly in the case of low alkali metal atom density [37]. The results of that analysis, however, are rather complex and are not transparent to easy interpretation. In order to interpret more easily experimental data in connection with atomic frequency standards applications, simpler analyses have been developed [24, 26]. In those analyses, a three-level model is also used, but the rate equations are solved approximately by means of a first-order analysis relative to optical coherence. The expressions obtained for the hyperfine resonance line shape, width, and amplitude are transparent and easy to interpret. The results can explain most experimental data in the case of an optically thin absorbing medium. The optical thickness is controlled by both the buffer-gas pressure, which broadens the absorption line, and the alkali-atom density, which influences the optical absorption. In practice, the temperature of operation ($T > 50^\circ\text{C}$ in the case of Rb, $T > 40^\circ\text{C}$ in the case of Cs) is such that the ensemble is optically thick, and a more elaborate approach using concepts developed in the study of the electromagnetically induced transparency (EIT) phenomenon [15] is required [38]. Furthermore, in the case where relatively intense radiation fields are used, it is found that the three-level model is not adequate [39]. The lower manifolds of an alkali-metal atom contain many energy levels and the Λ system is no longer closed as in the three-level model [40]. For example, when circularly polarized radiation is used, as required to observe the so-called ground-state field-independent 0–0 transition, atoms are optically pumped to a level not involved in the coherent population trapping phenomenon. They are transferred to that level, and trapped in it: they no longer contribute to the CPT resonance phenomenon. This effect has consequences on the observed signal amplitude. This effect is also encountered in several other experimental studies related to atom cooling [41–44] and absorption of laser radiation [45].

Reviews have been made of the basic physics of CPT [46] and of its use in high-resolution spectroscopy [19]. The present paper will concentrate on the use of CPT in connection with application to the field of atomic frequency standards. We will make a review of the progress made up to now on the implementation of frequency standards using CPT, in either the active or the passive mode, in beams as well as in closed cells containing a buffer gas. We will review the theoretical analysis developed up to now to interpret the results obtained experimentally. Finally, as a conclusion, we will provide an unbiased evaluation of the implementations realized up to now. The number of articles published on the subject of CPT is rather large. We will limit the present review to those articles most closely connected to the field of atomic frequency standards and useful in the interpretation of the results obtained in the implementation of those standards.

2 Coherent population trapping

2.1 The phenomenon

We will first establish the basic equations, describing the CPT phenomenon in an alkali-metal atom such as the ^{87}Rb isotope, and we will adapt those to various situations. To do so, we will assume the presence of two coherent radiation fields resonant with the transitions from the levels $F = 1$ and $F = 2$ of the ground state to one of the hyperfine levels of the excited P state. In practice it is best to choose level $P_{1/2}$, $F' = 2$ (D_1 radiation), since in that case the transition probability is the same for both transitions making the system symmetrical, avoiding direct optical pumping and simplifying the analysis [47]. The analysis can be easily adapted to other pairs of levels and to the case of other alkali-metal atoms. The scheme is illustrated in Fig. 1a.

In the scheme shown, only those transitions starting from the levels $m_F = 0$ of the ground state are shown, although the spectral width of the lasers generally used would allow transitions from other Zeeman levels. In all applications concerned, however, a small magnetic field of the order of $10\ \mu\text{T}$ is applied to the atomic ensemble and the other Raman resonances are well resolved. Consequently, a given Λ scheme may be selected to be resonant with only two of the ground-state levels. In the present case, the scheme starting at levels $m_F = 0$ is chosen since the positions of these levels are independent of the applied magnetic field in first order, a property desired in frequency standards applications. It is noted also that right hand circular polarization exciting $\Delta m_F = +1$ transitions is used. Left hand circular polarization can also be used. Circular polarization is required by the fact that transitions involving simultaneously $\Delta F = 0$ and $\Delta m_F = 0$ are forbidden. However, other Zeeman levels may play a role in the evolution of the system. Decay from the excited state takes place to all ground-state Zeeman sublevels due to spontaneous emission and due to atomic collisions in the case a buffer gas is used. Consequently, atoms may find a path to a Zeeman sublevel not involved in the Λ scheme. In such a case, the system is no longer closed and atoms may be trapped in a level such as $m_F = +2$ or $m_F = -2$, depending on the polarization used as in a classical optical pumping process [10]. Those atoms are lost for the CPT phenomenon. This phenomenon takes place

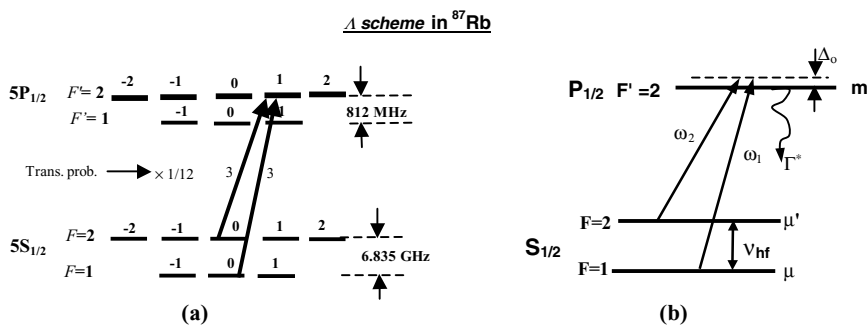


FIGURE 1 a Illustration of the lower energy levels manifold involved in the CPT excitation of the alkali-metal atom ^{87}Rb using circularly polarized radiation σ^+ . b Closed three-level model generally used to analyze the CPT phenomenon

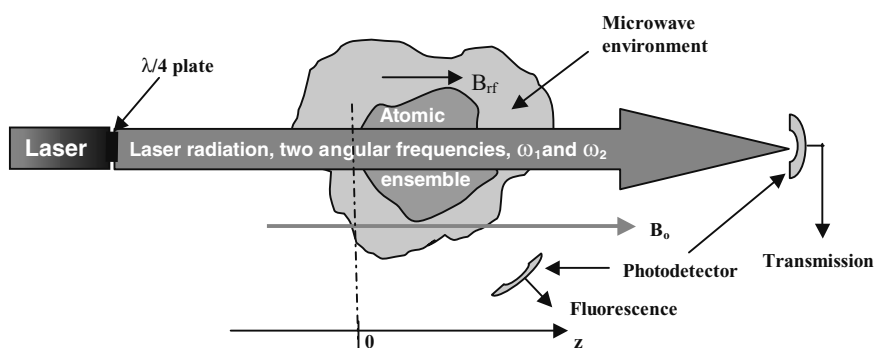


FIGURE 2 General configuration used in the development of the rate equations

in a buffer gas and becomes important at laser intensities corresponding to excitation rates comparable to or larger than the ground-state relaxation rates. Consequently, it is necessary to use a four-level system including a trap to explain some of the results obtained [39].

The analysis is best done in the density-matrix formalism. The general configuration shown in Fig. 2 is used to establish the rate equations. The atomic ensemble may be contained in a closed cell and imbedded in a buffer gas. In that case the populations of the levels within the ground state and the coherence that may exist at the hyperfine frequency relax towards equilibrium at rates γ_1 and γ_2 , respectively. On the other hand, if the atomic ensemble is an atomic beam, those rates may be assumed to be zero. The buffer gas also has important effects on the excited state, increasing the decay rate Γ^* of the P state by a factor that depends on its pressure. Consequently, the optical resonance line is homogeneously broadened to a large extent. At a buffer-gas pressure of about 20 Torr, the rate Γ^* is of the order of $3 \times 10^9 \text{ s}^{-1}$ as compared to a free space decay rate Γ (spontaneous emission) of the order of $3 \times 10^7 \text{ s}^{-1}$, as in a beam.

2.2 Basic equations

In the analysis the laser radiation is assumed to propagate in the same direction as the applied magnetic field. The electric component E_n of the two laser radiation fields is assumed to be of the form

$$E_n(\omega_n, z, t) = E_{on}(z) e_\lambda \cos(\omega_n t + \mathbf{k}_n \cdot \mathbf{r}) \quad (n = 1, 2), \quad (1)$$

where E_{on} is the amplitude of the laser radiation field component n at position z , ω_n is its angular frequency, \mathbf{k}_n is its

wave vector, e_λ is the polarization vector assumed the same for both radiation fields, and z is the distance traveled by the wave as measured from the entrance of the region containing the atomic ensemble. These two radiation fields may be produced from a single laser through bias-current modulation or by means of an electro-optic modulator. The two radiation fields may also be created by means of two phase-locked lasers with a frequency difference corresponding to the hyperfine frequency.

We introduce the optical Rabi angular frequencies ω_{R1} and ω_{R2} as a measure of the laser field intensity and of the transition probability:

$$\omega_{R1} = (E_1/\hbar) \langle \mu | \mathbf{e} \mathbf{r} \cdot \mathbf{e}_\lambda | m \rangle, \quad (2)$$

$$\omega_{R2} = (E_2/\hbar) \langle \mu' | \mathbf{e} \mathbf{r} \cdot \mathbf{e}_\lambda | m \rangle, \quad (3)$$

where e is the electronic charge, \hbar is Planck's constant over 2π , and $\langle i | \mathbf{e} \mathbf{r} | m \rangle$ is the electric dipole moment of the transition from level i to level m ($i = \mu$ or μ'). We assume that the ensemble is placed in an environment where a microwave field $B_{\mu w}(z, t)$ oscillating at angular frequency $\omega_{\mu w}$ may be present. This field, which may be created by the atoms themselves through stimulated emission, is assumed to be parallel to the dc magnetic field, a condition required for $\Delta m_F = 0$ transitions. In that condition the microwave field is assumed to have the form

$$\mathbf{B}_{\mu w}(z, t) = \mathbf{z} B_z(z) \sin(\omega_{\mu w} t + \phi), \quad (4)$$

where ϕ is its phase. The associated Rabi angular frequency describing the interaction of this field with the atomic ensemble is defined as

$$b(z) = \mu_z B_z(z) / \hbar, \quad (5)$$

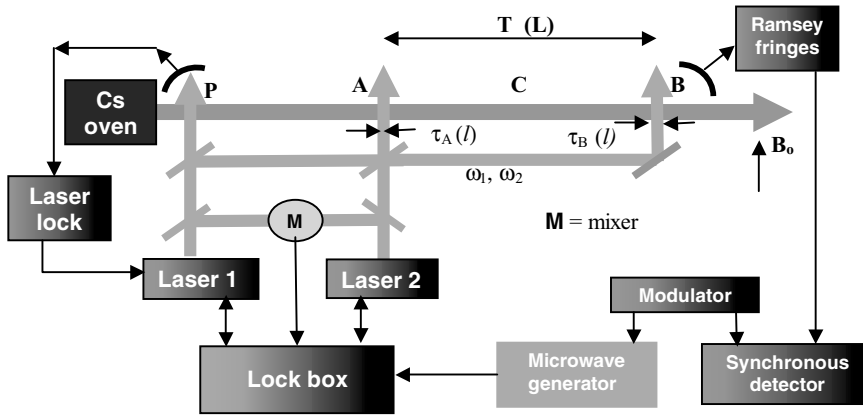


FIGURE 3 Alkali metal atomic beam frequency standard using CPT excitation and detection. B_0 is the magnetic induction applied parallel to the propagation vector k of the laser beams in interaction with the atomic beam

where μ_z is the atom magnetic moment. We define

$$\omega_{12} = \omega_1 - \omega_2. \quad (6)$$

The rate equations for the populations of the levels and for the coherence in the ground state are obtained from Liouville's equation:

$$\frac{\partial \rho}{\partial t} = \frac{1}{i\hbar} [H, \rho], \quad (7)$$

where ρ is a density-matrix element and H is the interaction Hamiltonian.

We expand this equation into its various terms. We assume a solution for the off-diagonal matrix elements of the form

$$\rho_{\mu\mu'}(z, t) = \delta_{\mu\mu'}(z, t) e^{i[(\omega_1 - \omega_2)t - (k_1 - k_2)z]}, \quad (8)$$

$$\rho_{\mu m}(z, t) = \delta_{\mu m}(z, t) e^{i[\omega_1 t - k_1 z]}, \quad (9)$$

$$\rho_{\mu' m}(z, t) = \delta_{\mu' m}(z, t) e^{i[\omega_2 t - k_2 z]}, \quad (10)$$

and the resulting equations for the three level system are

$$\frac{d}{dt} \rho_{mm} = -\omega_{R1} \text{Im} \delta_{\mu m} - \omega_{R2} \text{Im} \delta_{\mu' m} - \Gamma^* \rho_{mm}, \quad (11)$$

$$\begin{aligned} \frac{d}{dt} \rho_{\mu'\mu'} = & -\text{Im}(b e^{-i\phi}) \delta_{\mu\mu'} + \omega_{R2} \text{Im} \delta_{\mu' m} + \Gamma_{m\mu'}^* \rho_{mm} \\ & - (\gamma_1/2)(\rho_{\mu'\mu'} - \rho_{\mu\mu}), \end{aligned} \quad (12)$$

$$\begin{aligned} \frac{d}{dt} \rho_{\mu\mu} = & +\text{Im}(b e^{-i\phi}) \delta_{\mu\mu'} + \omega_{R1} \text{Im} \delta_{\mu m} + \Gamma_{m\mu}^* \rho_{mm} \\ & - (\gamma_1/2)(\rho_{\mu\mu} - \rho_{\mu'\mu'}), \end{aligned} \quad (13)$$

$$\begin{aligned} \frac{d}{dt} \delta_{\mu m} + (\Gamma^*/2 + i(\omega_1 - \omega_{m\mu})) \delta_{\mu m} = & + i(\omega_{R1}/2)(\rho_{mm} - \rho_{\mu\mu}) \\ & + i(b/2) e^{i\phi} \delta_{\mu' m} - i(\omega_{R2}/2) \delta_{\mu\mu'}, \end{aligned} \quad (14)$$

$$\begin{aligned} \frac{d}{dt} \delta_{\mu' m} + (\Gamma^*/2 + i(\omega_2 - \omega_{m\mu'})) \delta_{\mu' m} = & + i(\omega_{R2}/2)(\rho_{mm} - \rho_{\mu'\mu'}) \\ & + i(b/2) e^{-i\phi} \delta_{\mu m} - i(\omega_{R1}/2) \delta_{\mu\mu'}, \end{aligned} \quad (15)$$

$$\begin{aligned} \frac{d}{dt} \delta_{\mu\mu'} + [\gamma_2 + i(\omega_{12} - \omega_{\mu'\mu})] \delta_{\mu\mu'} = & i(b/2) e^{i\phi} (\rho_{\mu'\mu'} - \rho_{\mu\mu}) \\ & + i(\omega_{R1}/2) \delta_{m\mu'} - i(\omega_{R2}/2) \delta_{\mu m}, \end{aligned} \quad (16)$$

with the condition

$$\rho_{mm} + \rho_{\mu'\mu'} + \rho_{\mu\mu} = 1. \quad (17)$$

The above equations apply to a group of atoms having a given velocity. Doppler broadening of the optical interaction is of the order of 500 MHz. In a cell containing a buffer gas, as mentioned above, collisions cause optical line broadening of several hundreds of MHz and in that case homogeneous broadening represented in the equations by the decay rate Γ^* is assumed. It is also assumed that Dicke narrowing takes place at the microwave frequency corresponding to the hyperfine frequency of the ground state [48]. When the phenomenon is observed in an atomic beam, the experimental setup is such that the laser radiation traverses the beam at right angles, avoiding the first-order Doppler effect. Questions of the phase of the various fields are taken into account in the derivation when appropriate.

We will apply this set of equations to several cases representing the experimental approaches that have been studied towards the implementation of a frequency standard. The parameters in the above set of equations will be adjusted to the appropriate experimental situations encountered in those various approaches. The analysis can also be adapted easily to other alkali atoms through a proper adjustment of the frequencies, wavelengths, and other decay and relaxation parameters.

3 The two-zone atomic beam approach

The first reports of the use of CPT for implementing a frequency standard describe a laboratory system in which a beam of sodium atoms is excited by means of CPT at two zones separated by a distance L as shown in Fig. 3 [22, 49–52]. The approach simulates the standard Ramsey separated field technique used in classical Cs beam standards [23]. To implement this technique with CPT, two co-linear laser radiation fields at frequencies ω_1 and ω_2 are used. The light beam incorporating these two fields is made to cross at right angles the thermal alkali-metal atomic beam at two regions of space or zones separated by a distance L . The interaction in the first zone A, lasting for a time τ_A , places the atoms in a superposition state through the CPT phenomenon. The atoms emerge from zone A in a coherent state as after a $\pi/2$ pulse. These atoms evolve freely in space C in that superposition state for a time T ($T = L/\langle v \rangle$, where $\langle v \rangle$ is the average speed

of the atoms). They then enter into the second zone B where they interact with the same radiation fields for a time τ_B . First zone A acts essentially as the first branch of the Ramsey cavity in the classical approach. The interaction in the second zone, acting in a similar way and consisting of an excitation by radiation fields of a phase related to that existing in the first zone, enters into interference with the coherence carried by the atomic beam. The fluorescence emitted in this second zone reflects this interference phenomenon and shows up as Ramsey fringes as in the classical approach.

The main advantage that results in this CPT approach, also called Raman–Ramsey excitation, over the classical approach is the absence of a Ramsey double microwave interaction structure and of selector magnets. No state preparation in principle is required although zone P could be used for such a purpose. No microwave excitation is required and the whole system gains in simplicity. The atomic beam can be enclosed entirely in a sealed evacuated glass tube with a diameter of a few mm, and 10–15-cm long. In such an arrangement, the central fringe has the same width ($\sim 1/2T$) as in the classical approach using a similar Ramsey interaction length. The approach also gains a great deal in simplicity when compared to the optical pumping approach used for atom preparation and detection in combination with a microwave Ramsey interaction structure. In that case, the optical pumping is used solely to replace the selector magnets, and the Ramsey microwave interrogation structure is still required. In the CPT approach, preparation and interrogation are done in the same region of space and no microwave structure is needed.

3.1 Basic theory

Basic equations (8)–(17) describing the interaction with the atomic system apply, except that in the present circumstances there is no microwave field applied, and there is no buffer gas present. Consequently, $b = 0$ and the relaxation rates in the ground state γ_1 and γ_2 are both zero. In a beam, atoms are free, and the decay from the excited state takes place by spontaneous emission at the rate Γ . In order to obtain easily tractable expressions, we assume that $\omega_{R1} = \omega_{R2} = \omega_R$. Hemmer et al. [53] have solved the resulting set of equations and have obtained expressions for the fringe as observed in zone B and the phase associated with it. The calculations done in a mathematical context somewhat different from that used by Hemmer et al. are outlined in Annex A. The expression for the fringes is

$$P_{fl}(\text{zone B}) = (1 - \exp[-\Gamma\xi\tau_B/(1 + 3\xi)]) \times N\hbar\omega\{1 + (-1 + \exp[-\Gamma\xi\tau_A/(1 + 3\xi)]) \times |\sec[\phi_A]|\cos[\phi_A - T\Omega_\mu]\}, \quad (18)$$

while the phase of the atoms at the exit of zone A is given by

$$\tan[\phi_A] = \frac{\alpha^i}{\alpha^r} = \frac{\exp[-\Gamma\xi\tau_A](\rho_{\mu'\mu'} - \rho_{\mu\mu})_0 \sin[\Gamma\xi\delta_0\tau_A]}{1 - \exp\left[-\frac{\Gamma\xi\tau_A}{1+3\xi}\right]}. \quad (19)$$

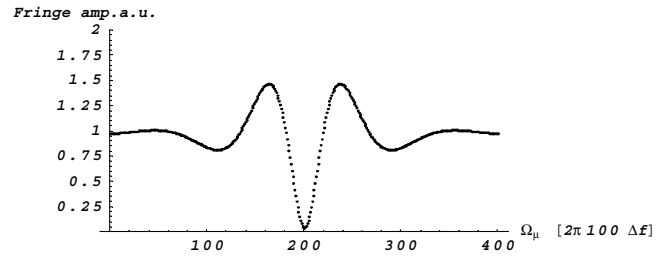


FIGURE 4 Ramsey fringe calculated for the CPT two-zone approach in an alkali-metal atomic beam

In those equations, N is the total number of atoms in interaction with the laser beam in zone B and $(\rho_{\mu'\mu'} - \rho_{\mu\mu})_0$ is the population difference of states μ' and μ at the entrance of zone A. The following definitions are also used:

$$\Omega_\mu = \omega_{12} - \omega_{\mu'\mu}, \quad (20)$$

$$\delta_0 = \frac{2\Delta_0}{\Gamma}, \quad (21)$$

$$\xi = \frac{\Omega_R^2/\Gamma^2}{1 + \delta_0^2}. \quad (22)$$

The phase shift is caused by the ac Stark effect taking place in zone A (light shift) and causes a frequency shift as in the classical Ramsey separated zone approach, although the physical origin of this phase shift is quite different. The times τ_A , τ_B , and T are functions of the atomic velocities. Consequently, the actual shape of the Ramsey fringe is obtained through an integration over all interaction times in the beam, whose spread is given by an altered Maxwell–Boltzmann distribution [21]:

$$f(\tau) = \frac{2}{\tau_0} \left(\frac{\tau_0}{\tau}\right)^5 e^{-(\tau_0/\tau)^2}. \quad (23)$$

This expression is normalized to unity upon integration over τ . For a ratio L/l equal to 100, numerical integration with $\Gamma = 3 \times 10^7 \text{ s}^{-1}$ gives a fringe shape as shown in Fig. 4.

The effect of the phase shift on the central fringe is to displace its center by the amount

$$\Delta\omega(\phi_A) = \phi_A/T. \quad (24)$$

This phase shift is referenced to the phase imbedded in the laser radiation and supported in the second zone. Its behavior as a function of detuning δ_0 is shown in Fig. 5 for several values of ω_R and a value of $\rho_{\mu'\mu'} - \rho_{\mu\mu}$ equal to 0.2. It has been averaged over atomic velocities using the same distribution as that used in the case of the fringe calculation, with $\Gamma = 3 \times 10^7 \text{ s}^{-1}$ and a ratio $L/l = 100$.

As is clearly seen in this graph, the dependence of the phase on tuning is much reduced around the value $\delta_0 = 50$, which corresponds to exact optical resonance in the axis origin chosen for the calculation. The reduction varies with Rabi frequency or laser intensity. This behavior appears essentially as an optical saturation effect, although the excited state m never becomes much populated even for $\omega_R = 0.25\Gamma$.

With the intent of making more transparent the physics involved in this two-zone CPT setup, we have limited the above analysis to the case of equal intensities for the laser radiation fields at ω_1 and ω_2 . The problem of unequal intensities is more

complex. However, it is shown that the general behavior regarding phase shift is not much dependent on this asymmetry [53].

3.2 Experimental results

Laboratory setups using such an approach have been implemented with the alkali atoms Na and Cs [22, 54]. In the case of sodium, a dye laser was used as the source of the two radiation fields, while for cesium diode lasers were used. The results confirm the observation of Ramsey fringes in the fluorescence of the second zone with a shape in agreement with that shown above.

3.2.1 Frequency stability. In sodium, with a distance $L = 15$ cm between the interaction zones, a fringe line width at half maximum of 2.2 kHz was obtained experimentally. On the other hand, a signal to noise ratio of 4500 for 1-s averaging time was also measured. The expected frequency stability for such a setup in the limit of shot noise was calculated to be $5 \times 10^{-10} \tau^{-1/2}$. The measured frequency stability confirmed this evaluation [22, 51]. In the case of Cs, a signal to noise ratio of 1800 was observed for an averaging time of 1 s. It was projected that the measured fringe width (1 kHz) and this signal to noise ratio translated into a frequency stability of $6 \times 10^{-11} \tau^{-1/2}$ [54].

3.2.2 Frequency shifts. The ac Stark phase shift: the phase shift was measured for different values of the optical Rabi frequency and various values of the ground-state population difference at the entrance of the first zone [53]. The results are in general agreement with the model developed and summarized above, the phase shift introduced by the first interaction zone following the trend shown in Fig. 5. It is found that for certain adjustments of the parameters, such as large pumping rates, the slope of the phase shift as a function of detuning δ_0 changes sign. This behavior was explained by means of differences between the decay rates from the excited state to various levels of the ground state. It should be mentioned, however, that the actual variation of ϕ_A with δ_0 is a very sensitive function of the Rabi frequency ω_R and shows a complicated behavior regarding the sign of the slope at large values of the Rabi frequency, as shown in Fig. 5. Hemmer et al. [53] have

also evaluated that the minimum slope observed in their setup (Na beam) led to a frequency shift of the order of 2×10^{-11} for a laser detuning of 0.01Γ , corresponding to a detuning of the order of 300 kHz. Recent theoretical work has considered the multiplicity of levels entering into interaction with the laser radiation [55].

Other frequency shifts: there are several other frequency shifts present in the approach proposed. In particular, a frequency shift may be present if a phase shift is introduced physically through a difference in path lengths between the two radiation beams before entering the interaction regions. Such a phase shift was commented upon in Ref. [56]. It has also been observed [53]. Other important frequency shifts may be caused by misalignment of the ω_1 and ω_2 radiation beams, phase shifts due to laser polarization, atomic beam or laser beam misalignment, and overlapping of Ramsey fringes. The importance of these shifts has been evaluated and, although they are not negligible, it is believed that they would not cause a major impediment in the practical realization of an operational frequency standard with useful properties [51].

4 Sealed cell with a buffer gas in continuous mode: passive frequency standard

An experimental arrangement using a sealed cell is shown in Fig. 6. The setup shown can be used either to observe the CPT phenomenon through the transmitted radiation or to implement a frequency standard by closing the feedback loop by means of appropriate modulation and synchronous detection. It is also general practice to include in such a setup a second feedback loop for locking the laser wavelength to the optical absorption in the cell. We assume that a buffer gas such as N_2 is used. Collisions with this molecule have the property of quenching the fluorescence. This is a desirable property since fluorescence photons emitted at random would cause optical pumping, resulting in a loss of coherence in the ensemble. The use of such a gas prevents of course detection of the resonance CPT phenomenon by means of fluorescence.

As is readily observed in Fig. 6, no microwave field is applied and no microwave cavity is required. This is an advantage of the approach over the classical intensity optical pumping approach (IOP) that uses the double microwave-optical resonance technique. The two approaches have been compared in some detail in the same cell and conclusions

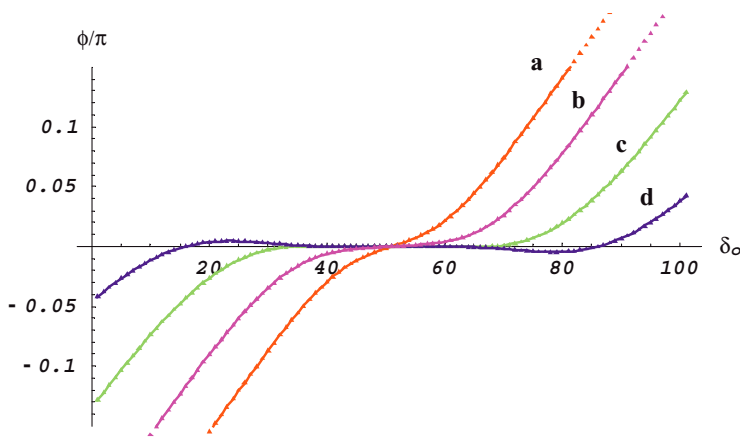


FIGURE 5 Phase shift affecting the Ramsey fringe in the case of a two-zone CPT approach in an atomic beam. The phase shift is averaged over velocities in zone A as for the Ramsey fringes. The parameters used for this graph are $\Gamma = 3 \times 10^7 \text{ s}^{-1}$, $\tau_A = 10^{-5} \text{ s}$, and $\rho_{\mu'\mu'} - \rho_{\mu\mu} = 0.2$. **a** $\omega_R = 0.1\Gamma$, **b** $\omega_R = 0.15\Gamma$, **c** $\omega_R = 0.2\Gamma$, **d** $\omega_R = 0.25\Gamma$. The optical resonance condition corresponds to $\delta_0 = 50$ on the axis chosen

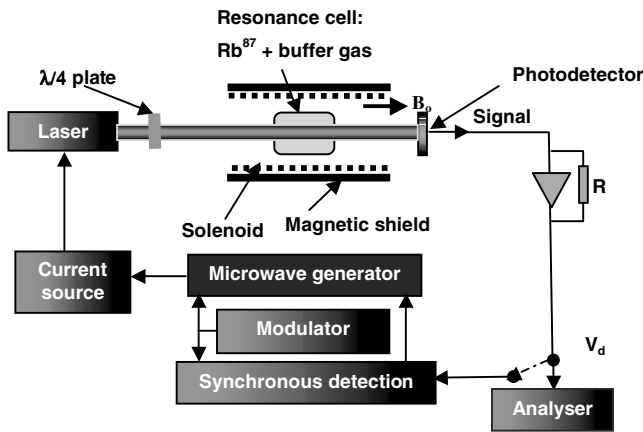


FIGURE 6 Experimental arrangement used either to observe the CPT phenomenon in transmission or to implement a passive frequency standard

have been reached regarding specific advantages of CPT over IOP in implementing a passive closed cell atomic frequency standard [57, 58]. The microwave Rabi angular frequency b is thus set equal to zero in Eqs. (11)–(17). The solution of this set of equations can be obtained exactly [37]. However, as mentioned above, such a solution is rather complex and is not transparent to easy interpretation. It is best to perform approximations in order to obtain some insight into the physical phenomena taking place and to evaluate the importance of the various parameters in the final implementation of a frequency standard.

4.1 Signal amplitude and line width

4.1.1 Homogeneous three-level model. In practice, the parameter measured in Fig. 6 is the light intensity at the exit of the cell. Actually, the CPT phenomenon is observed as an increase of transparency of the cell, or a reduction in power absorbed, at exact resonance. The power absorbed by slice dz of the cell is given by

$$\Delta P_{\text{abs}}(z) = n\hbar\omega_1\Gamma^*\rho_{\text{mm}} dz, \quad (25)$$

where n is the alkali-metal density. The energy absorbed is given back either as fluorescence or to the buffer gas vibration modes when a quenching gas such as N_2 is used. Consequently, a measure of transparency is obtained from the change of the population of the excited state ρ_{mm} upon CPT resonance. The value of ρ_{mm} is given by Eq. (11) in stationary state. In the case of low Rb density, the absorption is small and the system may be considered homogeneous. As an approximation, we may then assume that the density-matrix elements are constant throughout the cell. If the sidebands at ω_1 and ω_2 have the same amplitude and the laser is exactly tuned to the optical transition, the populations of the two ground levels remain equal, that is $\rho_{11} = \rho_{22}$, and straightforward algebra gives the excited-state population as

$$\rho_{\text{mm}} = \frac{\omega_{\text{R}}^2}{\Gamma^*2} \{1 + 2\delta_{\mu\mu'}^{\text{r}}\}, \quad (26)$$

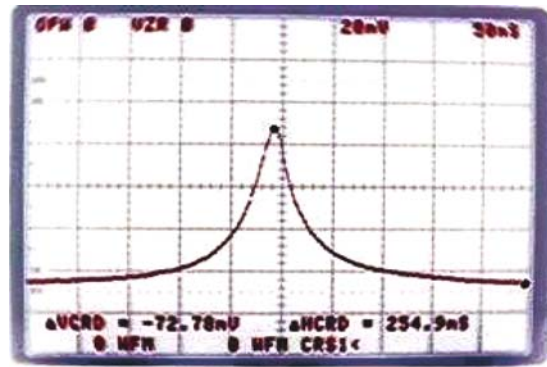


FIGURE 7 Experimental transmission CPT signal in a small cell in ^{87}Rb . In that particular recording made in an Ar/N_2 mixture with a pressure ratio of ~ 1.5 and at a temperature of about 65°C , the line width is of the order of 500 Hz and the contrast is about 5%

where $\delta_{\mu\mu'}^{\text{r}}$ is the real part of the coherence created in the ground state by the CPT phenomenon and is given by

$$\delta_{\mu\mu'}^{\text{r}} = -\frac{(\omega_{\text{R}}^2/2\Gamma^*)(\gamma_2 + \omega_{\text{R}}^2/\Gamma^*)}{(\gamma_2 + \omega_{\text{R}}^2/\Gamma^*)^2 + \Omega_{\mu}^2}, \quad (27)$$

with

$$\Omega_{\mu} = \omega_1 - \omega_2 - \omega_{\mu'\mu}. \quad (28)$$

The transmission shows a sharp increase at resonance when $\omega_1 - \omega_2 = \omega_{\mu'\mu}$. A typical experimental signal is shown in Fig. 7.

This CPT transmission resonance signal has a Lorentzian shape and has all the properties of the ground-state hyperfine resonance, as in the case of the double-resonance technique used in standards based on intensity optical pumping [58]. The width of the resonance line is given by

$$\Delta\nu_{1/2} = \frac{(\gamma_2 + \omega_{\text{R}}^2/\Gamma^*)}{\pi} \quad (29)$$

and is proportional to the laser radiation intensity. On the other hand, in this closed three-level model, the ensemble becomes totally transparent for a light intensity such that $\omega_{\text{R}}^2/\Gamma^*$ becomes much larger than the relaxation rate γ_2 .

This simple homogeneous model gives some insight into the behavior of the system and the importance of the sizes of the parameters. Later on, we will call $\omega_{\text{R}}^2/2\Gamma^*$ a pumping rate. For a Γ^* of $3 \times 10^9 \text{ s}^{-1}$ and a γ_2 of 1000 s^{-1} , typical values encountered in practical setups for a cell volume of a few cm^3 and a buffer-gas pressure of the order of 2 kPa (15 Torr), the Rabi angular frequency required to double the line width is $1.7 \times 10^6 \text{ s}^{-1}$. The laser intensity required for providing such a Rabi frequency is of the order of 10–100 $\mu\text{W}/\text{cm}^2$, depending on the laser radiation spectral width. It is also readily seen that in equilibrium, using these values, the population ρ_{mm} of the excited state does not exceed 3×10^{-7} , a value much smaller than that of the ground state.

4.1.2 Inhomogeneous model with a trap. The previous model, although providing the basic physics behind the CPT phenomenon for implementing a frequency standard, does not represent completely the experimental situation. First, optical absorption is not negligible and the ensemble at normal

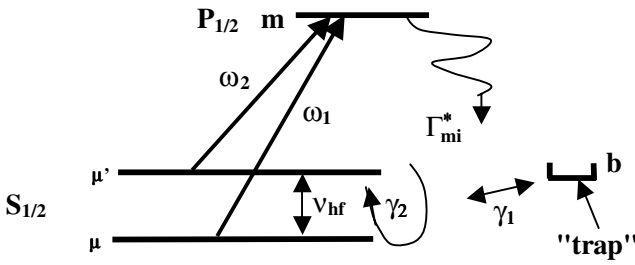


FIGURE 8 Four-level model used in the analysis to take into account the trapping property of the levels not involved in the Λ scheme and not excited by the laser radiation under circular polarization

temperatures of operation ($\sim 60^\circ\text{C}$ for Rb) is optically thick. The system is no longer homogeneous. Furthermore, the system includes several energy levels and is not closed. In particular, atoms excited to the P state under circular polarization (σ^+ or σ^-) and falling into either level $m_F = +2$ or level $m_F = -2$ are trapped in those levels for a time of the order of $1/\gamma_2$ and are lost for the CPT phenomenon involving the $m_F = 0$ levels. This effect may be accounted for by simply introducing a fourth level into the three-level model as shown in Fig. 8 [39].

All of Eqs. (11)–(16) stay the same except that we now have an added equation taking into account decay from level m to level b :

$$\frac{d}{dt}\rho_{bb} + (\rho_{bb} - 1/3)\gamma_1 = \Gamma_{mb}^*\rho_{mm}, \quad (30)$$

with

$$\rho_{\mu\mu} + \rho_{\mu'\mu'} + \rho_{bb} + \rho_{mm} = 1. \quad (31)$$

We assume that ρ_{mm} always stays very small and that the equilibrium value of all ground-state levels is $1/3$. In order to take into account the inhomogeneous character of the ensemble, it is required to obtain a relation between light intensity and position in the cell. This is done in the following way.

This coherent laser radiation field interacts with the ensemble and creates a polarization P_n . The field E_n and the polarization P_n are connected by the relation [21]

$$\frac{\partial^2 E_n}{\partial z^2} - \frac{1}{c^2} \frac{\partial^2 E_n}{\partial t^2} = \mu_0 \frac{\partial^2 P_n}{\partial t^2}, \quad (32)$$

where c is the speed of light and μ_0 is the permeability of free space. On the other hand, the polarization is given by

$$P = n\text{Tr}(\rho P_{\text{op}}), \quad (33)$$

where n is the Rb density and P_{op} the equivalent quantum-mechanical operator of the classical electrical polarization. In that expression ‘Tr’ means the trace of the product of the two matrices ρ and P_{op} . After some algebra, assuming a stationary state and making the adiabatic approximation, one obtains

$$\frac{\partial E_n}{\partial z} = \left(\frac{n\omega_n d_{ij}}{c\epsilon_0} \right) \text{Im}\delta_{ij}(z), \quad (34)$$

where ω_n is the laser sideband angular frequency, ϵ_0 the permittivity of free space, and d_{ij} the Rb atom electric dipole moment for transition i to j . d_{ij} contains the appropriate information on the transition probabilities of the transitions involved. $\text{Im}\delta_{ij}$ is the imaginary part of the optical coherence

(Eqs. (14) and (15)) created in the system by the laser radiation. The problem thus reduces to that of evaluating the value of δ_{ij} in stationary state. To simplify the calculation, we assume that the two radiation fields have equal intensities. Since we do not know the dynamics of the quenching by the buffer gas, we assume also that the decay rates from the excited state to all levels of the ground state are equal:

$$\Gamma_{m\mu}^* = \Gamma_{m\mu'}^* = \Gamma_{mb}^* = \Gamma^*/3. \quad (35)$$

Since the fractional population ρ_{mm} of the excited state is always small ($< 10^{-6}$) relative to that of the ground levels, we assume that, in equilibrium, in the absence of radiation, the ground-state levels have equal populations:

$$\rho_{\mu'\mu'}(\text{eq.}) = \rho_{\mu\mu}(\text{eq.}) = \rho_{bb}(\text{eq.}) = \frac{1}{3}. \quad (36)$$

Using Eqs. (2) and (3), Eq. (34) can be transformed readily into

$$\frac{\partial \omega_R}{\partial z} = \alpha \text{Im} \delta_{\mu\mu}, \quad (37)$$

where α is the absorption coefficient and is given by

$$\alpha = \left(\frac{\omega}{c\epsilon_0 \hbar} d_{\mu\mu}^2 \right) n. \quad (38)$$

The imaginary part of $\delta_{\mu\mu}$ is obtained from the rate equations at equilibrium. We assume that the laser is tuned to the optical transition and that the populations of the two ground levels contributing to the CPT phenomenon remain equal. Making the adiabatic approximation in which one assumes that the excited-state population and coherence follow the slow evolution of the ground state, one obtains

$$\text{Im} \delta_{\mu\mu} = -\frac{\omega_R}{\Gamma^*} \left(\frac{1}{3} - \frac{(2/9)(\Gamma_p/\gamma_1)}{1 + (2/3)(\Gamma_p/\gamma_1)} + \delta_{\mu\mu}^r \right), \quad (39)$$

where

$$\delta_{\mu\mu'} = \frac{-(2/3)\Gamma_p(\gamma_2 + 2\Gamma_p) + (4/9)\frac{\Gamma_p^2(\gamma_2 + 2\Gamma_p)}{\gamma_1(1 + 2\Gamma_p/3\gamma_1)}}{(\gamma_2 + 2\Gamma_p)^2 + (\omega_{12} - \omega_{\mu'\mu})^2} + i \frac{\left((2/3)\Gamma_p - (4/9)\frac{\Gamma_p^2}{\gamma_1(1 + 2\Gamma_p/3\gamma_1)} \right) (\omega_{12} - \omega_{\mu'\mu})}{(\gamma_2 + 2\Gamma_p)^2 + (\omega_{12} - \omega_{\mu'\mu})^2} \quad (40)$$

and

$$\rho_{bb} = \frac{1}{3} + \frac{(4/9)(\Gamma_p/\gamma_1)}{1 + (2/3)(\Gamma_p/\gamma_1)}. \quad (41)$$

In those equations, to simplify writing, we have defined the pumping rate, a function of position in the cell, as

$$\Gamma_p(z) = \frac{\omega_R^2(z)}{2\Gamma^*}. \quad (42)$$

In order to obtain the value of the radiation intensity at the exit of the cell, Eq. (37) needs to be solved with $\text{Im}\delta_{\mu\mu}$ and $\delta_{\mu\mu'}^r$ given by Eqs. (39) and (40). Unfortunately, due to the complexity of the right-hand side, Eq. (37) cannot be solved analytically and a numerical approach is required in which $\omega_R^2(z)$ is evaluated at the exit of the cell, that is $z = L$.

In view of the form of $\delta_{\mu\mu'}$, the resonance line shape is assumed to be Lorentzian with a width given by

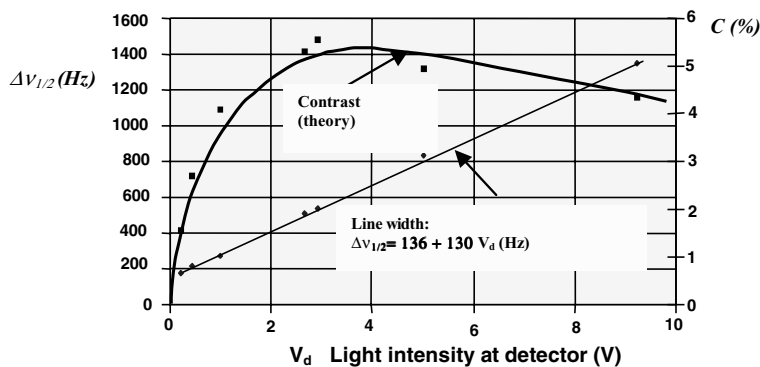


FIGURE 9 CPT contrast and line width in a ^{87}Rb cell containing an Ar–N₂ buffer-gas mixture and operated at 75°C. The points are experimental and the solid curves are theoretical

$$\Delta\nu_{1/2} = (1/\pi) (\gamma_2 + \omega_R^2(z=L)/\Gamma^*), \quad (43)$$

where γ_2 is the relaxation rate in the absence of laser radiation or $\omega_R = 0$. γ_2 includes several mechanisms such as relaxation by diffusion to the cell walls, relaxation by collisions with the buffer-gas molecules, and spin-exchange interaction between Rb atoms [21].

4.2 Practical implementation

4.2.1 Frequency stability. In the implementation of a passive frequency standard based on the CPT phenomenon, the frequency of the microwave generator used to modulate the laser frequency is locked to the center of the hyperfine resonance line. This may be done by modulating the frequency of the microwave generator at a low frequency and using synchronous detection to create an error signal. If the amplitude of this modulation is of the order of one-half of the resonance line width, the short-term frequency stability in the limit of shot noise is given approximately by [59–61]

$$\sigma(\tau) = \frac{K}{4\nu_{\text{hf}}} \sqrt{\frac{e}{I_{\text{bg}}}} \frac{1}{q} \tau^{-1/2}, \quad (44)$$

where K is a constant that depends on the type of modulation used and is of the order of 0.2, ν_{hf} is the hyperfine frequency, e is the charge of the electron, I_{bg} is the background current created by the residual transmitted radiation reaching the photodetector, τ is the averaging time, and q is a quality figure defined as the ratio of the contrast C to the line width $\Delta\nu_{1/2}$:

$$q = C/\Delta\nu_{1/2}. \quad (45)$$

The contrast C is defined as the CPT signal intensity divided by the background intensity. To obtain best frequency stability, it is thus important to maximize contrast and to minimize line width. In practice, the laser spectrum is affected by amplitude and frequency fluctuations, which are additional sources of noise affecting frequency stability, and the limit of shot noise given above is not reached. For example, the amplitude noise, characterized by the relative intensity noise (RIN) parameter [62], adds directly to shot noise. For amplitude noise, Eq. (44) becomes

$$\sigma(\tau) \approx \frac{1}{\sqrt{2}} \frac{(\text{RIN})^{1/2}}{4q \nu_{\text{hf}}} \tau^{-1/2}. \quad (46)$$

In such a case, it is also important to maximize the quality figure q . On the other hand, laser frequency fluctuations are transformed into amplitude fluctuations through various resonance mechanisms in the atomic ensemble and contribute to additional noise [63, 64].

The signal amplitude is a function of Rb density and pumping rate. A typical experimental result is shown in Fig. 9 for a cell containing a buffer-gas mixture of argon and nitrogen in the pressure ratio of 1.4 at 10.5 Torr.

The solid curve through the experimental points is a plot of a numerical integration of Eq. (37) using the four-level model developed above. The free parameter used in this plot is the maximum contrast observed. It is seen that the maximum contrast is limited to a value of the order of 5%. This is due to the fact that in ^{87}Rb only two levels out of eight in the ground state contribute to the CPT phenomenon, the other levels contributing individually to optical absorption. Furthermore, in modulating the laser through the bias current, many sidebands are produced which contribute to the background light intensity. It is possible to obtain a larger contrast by raising the cell temperature, thereby increasing Rb density and optical absorption. The contrast maximum is then observed at a larger light intensity. An undesired side effect is an increase in line width due to increased laser radiation broadening and spin-exchange interaction. In practice, the optimum operating condition giving a maximum quality figure q is determined experimentally.

The behavior of the line width is also shown in Fig. 9 as a function of light intensity. The result confirms the linear dependence of the line width on light intensity. It is used to calibrate the system in terms of Rabi frequency by means of Eq. (43). The four-level model was further verified by applying it to an ensemble at several other temperatures. It was found to agree well with the experimental data [39].

It may be pointed out that the standard three-level model predicts a contrast that increases with Rb density and laser radiation intensity, which is not in agreement with the experimental data that shows a maximum in response to laser intensity. The maximum is caused by the fact that the trapping of atoms in level $m_F = 2$ becomes important at radiation intensities larger than the relaxation rate in the ground state. Several approaches have been suggested to avoid the effect of trapping levels using push–pull optical pumping [65], counter-propagating waves [66, 67], or co-linear, so-called lin-per-lin polarization, laser beams [68]. These techniques make possible an increase in contrast and may be useful when small cells

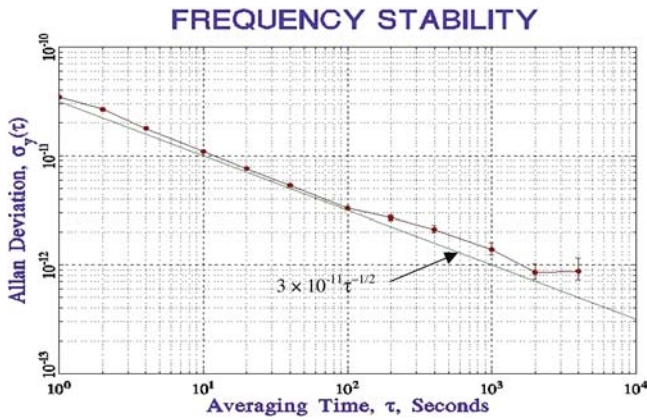


FIGURE 10 Frequency stability of a CPT frequency standard using a small cell (a few cm^3), a VCSEL as the laser pumping source, and a totally digital electronics approach for accomplishing the wavelength and frequency lock of the laser wavelength and microwave frequency to the atomic resonances (Kernco, model V01 [27, 28])

are used. However, they add complexity to the overall design of the optical system.

A totally autonomous frequency standard has been implemented using the basic approach shown in Fig. 6 [27, 28]. The alkali-metal atom used is ^{87}Rb and the buffer gas is a mixture of Ar and N_2 in a pressure ratio of about 1.5. The cell is a glass enclosure of a few cm^3 in volume and the radiation source is a vertical cavity surface emitting laser (VCSEL) modulated in frequency at 3.4 GHz. The contrast observed at the optimum operating point is of the order of 5% and the line width is somewhat less than 500 Hz. The electronic servo systems are entirely digital. The unit in its present stage of development has a volume of 125 cm^3 . The frequency stability obtained is of the order of $3 \times 10^{-11} \tau^{-1/2}$ and reaches levels below 10^{-12} at an averaging time of the order of 2000 s, as shown in Fig. 10.

4.2.2 Frequency shifts. As in the standard IOP double-resonance approach there are many frequency shifts that are present in such an implementation. These include magnetic field shifts, buffer-gas shifts, and light shifts. Although they are well known and do not cause a major problem, instability in these shifts may affect frequency stability in the medium- and long-term regions of averaging times.

Magnetic field shift: a magnetic field is required to provide an axis of quantization to the system and a reference axis for laser radiation polarization. The magnetic field removes Zeeman degeneracy in the ground state. The $m_F = 0$ sublevels are shifted quadratically, causing a shift of the hyperfine frequency according to [21]

$$\Delta\nu_B(^{87}\text{Rb}) = 575.14 \times 10^8 B_0^2 \text{ Hz}, \quad (47)$$

where B_0 is the magnetic induction in tesla (T). This field is generally created by means of a solenoid inside a magnetic shield. It is of the order of a few tens of μT . The current driving this field and the shielding factor are made compatible with the frequency stability desired. It should be mentioned that a magnetic field is required in all CPT implementations, in either the beam or the cell approach, and that the same requirements as those just mentioned apply.

Buffer-gas shift and temperature coefficient: the buffer gas causes a frequency shift. This shift is proportional to the buffer-gas density or, in a sealed cell, to its pressure P . Furthermore, this shift is temperature sensitive. The hyperfine frequency is shifted by [21]

$$\Delta\nu = P(\beta + \delta\Delta T + \gamma\Delta T^2), \quad (48)$$

where β is the pressure coefficient, δ is the linear temperature coefficient, and γ is the quadratic temperature coefficient. Two buffer gases widely used are nitrogen and argon that have opposite pressure and temperature coefficients. In that case the coefficients of Eq. (48) are combinations of the individual buffer-gas coefficients. When mixed in the ratio of pressures $R = P_{\text{Ar}}/P_{\text{N}_2} \sim 1.5$ the linear temperature coefficient is nearly canceled, and is of the order of $10^{-10}/^\circ\text{C}$. However, due to the presence of the quadratic term in Eq. (48), the residual coefficient is a function of the temperature of operation and can be minimized by appropriate adjustment of the ratio R for the desired temperature of operation [69]. On the other hand, due to uncertainties in the cell's filling pressure and the large buffer-gas frequency shift involved ($\sim 200 \text{ Hz per Torr}$), CPT units using the sealed-cell approach need to be calibrated and cannot be used as primary frequency standards.

Light shift: a frequency shift that has caused a major problem in the classical IOP approach using laser optical pumping is the light shift [70, 71]. Fortunately, this shift appears to be well under control in CPT. In the case of frequency-modulated lasers, this is due to the fact that for equal amplitudes, the first sidebands' radiation fields displace both ground-state levels by the same amount. On the other hand, the total light shift introduced by all sidebands disappears for certain modulation conditions. This question has been studied in some detail [72–74]. The total sidebands' light shift is given by

$$\frac{\Delta\omega_{\text{LS}}}{\omega_{\mu'\mu}} = \left(\frac{\omega_{\text{RL}}}{\omega_{\mu'\mu}}\right)^2 \left\{ \Theta(m) + \xi(m) \left(\frac{\Delta_0}{\omega_{\mu'\mu}}\right)^2 \right\}, \quad (49)$$

where it is recalled that Δ_0 is the laser detuning. The coefficients $\Theta(m)$ and $\xi(m)$ are given by the following expressions and are plotted in Fig. 11 as a function of the index of modulation m :

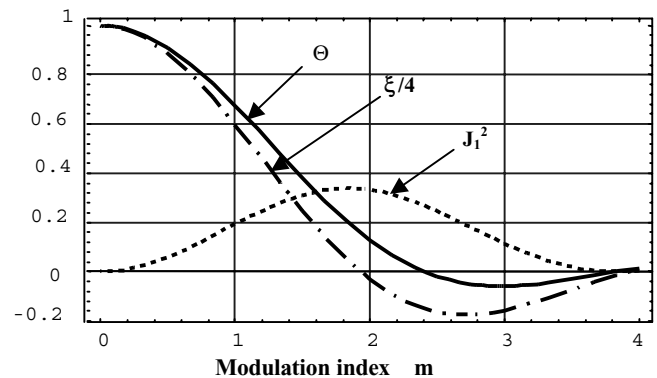


FIGURE 11 Variation of the light-shift coefficients with modulation index in the case where the first sidebands J_{1+} and J_{1-} are used to excite the CPT phenomenon ($p = 2$) [73]

$$\Theta(m) = J_0^2(m) + (1/2)J_{p/2}^2(m) - 2 \sum_{n=1 \neq p/2}^{\infty} J_n^2(m) \left(\frac{p^2}{(2n)^2 - p^2} \right), \quad (50)$$

$$\xi(m) = 4J_0^2(m) - 8 \sum_{n=1 \neq p/2}^{\infty} J_n^2(m) \frac{12n^2 + p^2}{((2n)^2 - p^2)^3} p^4. \quad (51)$$

In these expressions J_i is a Bessel function and p is an even integer defined as the ratio of the hyperfine frequency ω_{hf} to the laser modulation frequency ω_m . When p is set equal to 2, the two first sidebands J_{1+} and J_{1-} on each side of the carrier are used in the CPT Λ scheme and, in the case of ^{87}Rb , ω_m is $2\pi \times 3.41 \times 10^9 \text{ s}^{-1}$.

As is readily observed, the main component of the light shift, called the power shift and given by the coefficient $\Theta(m)$, vanishes at a laser modulation index, $m = 2.4$. This is due to the fact that the sidebands created in the modulation process

create light shifts that compensate each other. A typical experimental result is shown in Fig. 12 for the unit just mentioned [27, 28].

These results show that the clock frequency becomes independent of laser intensity for a modulation index of ~ 2.4 , as predicted. On the other hand, the quadratic part of the light shift given by coefficient $\xi(m)$ is of the order of 10^{-14} per $(\text{MHz})^2$ of laser detuning from optical resonance and is negligible in most circumstances [73].

4.2.3 Line shape. In the analysis just presented, the amplitudes of the two sidebands J_{1+} and J_{1-} were assumed equal. Furthermore, it was assumed that the laser is tuned exactly to the optical transition. Studies of the shape and of the center frequency of the hyperfine resonance as observed in transmission have been made for the case when these two conditions are not satisfied [75]. The problem was analyzed for the case of a three-level model in an optically thin sample. A numerical solution of the rate equations showed that when the two conditions are not satisfied, the line shape is no longer Lorentzian, as is shown in Fig. 13a. However, the minimum of

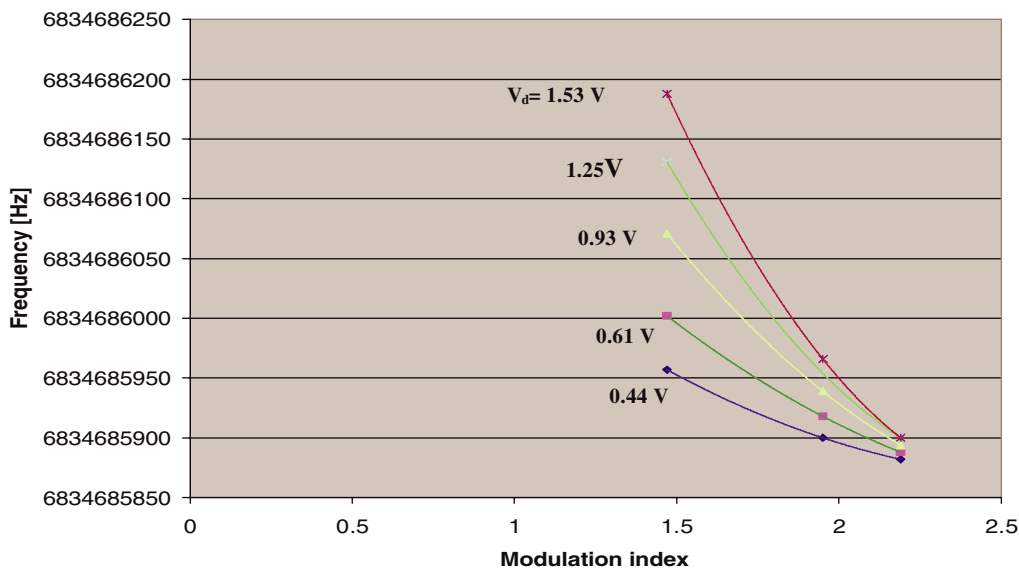


FIGURE 12 Light shift observed in the compact unit described in the text as a function of the modulation index of the laser for various radiation intensities [27, 28]. The numbers associated with the various curves are light intensities as measured at the photodetector in Fig. 6

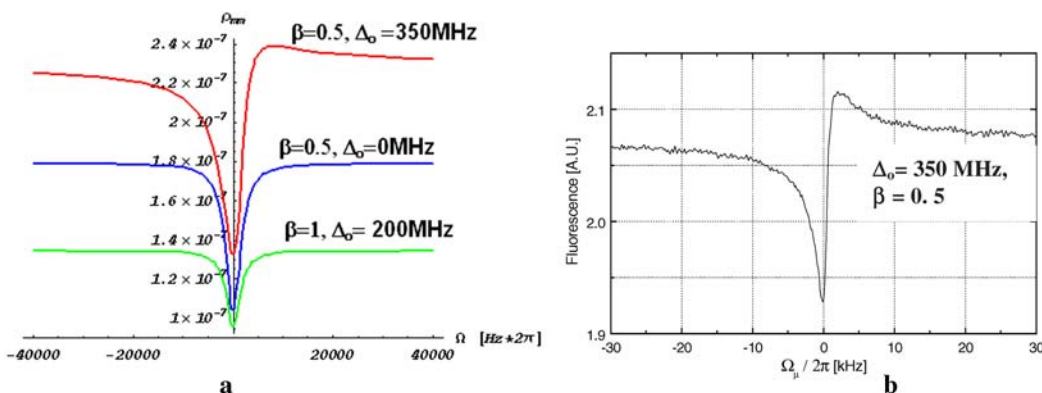


FIGURE 13 Line shapes in the case of laser detuning and unequal sidebands. **a** Theoretical; β stands for the ratio ω_{R1}/ω_{R2} and Δ_0 is the laser central frequency detuning defined in Fig. 1b. **b** Experimental [77]

the resonance line is not displaced in the process. This effect is observed experimentally, as is shown in Fig. 13b.

The question of the effect of the laser light beam transverse variation on the shape of the CPT resonance line was also addressed [75, 76]. The line shape is altered because the pumping rate $\omega_R^2/2\Gamma^*$ is a function of radial position across the laser beam. In the case of low pumping rates, it is found that the line shape remains Lorentzian while in the case of large pumping rates the line shape becomes sharper than a Lorentzian, although it remains symmetrical.

It is interesting to point out that the four-level model with a trap, used above to explain the behavior of the CPT transmission resonance line contrast in ^{87}Rb , may also be used to analyze the shape of the absorption spectrum for the case of an unmodulated laser radiation field. In practice, it is found that the recorded shape of the optical absorption for the D1 line is a function of polarization and light intensity. This is due to the fact that upon slow sweeping of the laser wavelength across the absorption line, optical pumping takes place, with various energy levels acting as traps. An analysis similar to that done above but with monochromatic radiation was done for ^{87}Rb . The results are reported in Annex B and are found to be in agreement with the observed absorption spectra. These results validate to some extent the four-level model used above to explain the contrast observed in the CPT transmission resonance line.

Aside from the early work reported on ^{87}Rb and ^{133}Cs [24, 25], work has also been done using ^{85}Rb [78, 79]. In the last case, the hyperfine frequency is 3.035 GHz. An edge-emitter diode was used, modulated at that frequency. The carrier J_0 and one of the first sidebands J_1 were used to generate the two laser frequencies identified as ω_1 and ω_2 in Fig. 1. Argon and neon were used as buffer gases. A CPT hyperfine resonance line width at room temperature of the order of 20 Hz for zero light intensity was obtained. This compares well to a line width of 10 Hz measured in the dark in such buffer gases at room temperature by means of the pulsed stimulated emission technique [80]. In that case a frequency generator locked to the CPT resonance line gave a frequency stability of $3.5 \times 10^{-11} \tau^{1/2}$ for $1 \text{ s} < \tau < 2000 \text{ s}$.

4.2.4 Other approaches. Cesium has also been used in bench setups to demonstrate the possibility of making a small optical package [25, 81, 82]. Recently, the implementation of an optical package using a semiconductor substrate as the container has been reported [35, 36]. The intention is the implementation of an integrated unit including control electronics on the same substrate. Since the cell itself is very small (\sim a few mm^3), diffusion to the walls causes a large CPT resonance line broadening unless a large buffer-gas pressure is used, unfortunately affecting signal amplitude. In one particular setup using ^{87}Rb the arrangement was 12 mm^3 with a neon–argon buffer-gas mixture with respective pressures of 24 and 11 kPa. In order to obtain a contrast comparable to that obtained in cells with a larger volume, such as that mentioned above, optical absorption was raised by running the cell at 125°C . At such a temperature, the Rb density is very high and spin-exchange interaction becomes important causing line broadening. Furthermore, in order to obtain good resonance line contrast, a high laser intensity was required also causing a large broad-

ening of the resonance line. The resulting line width was of the order of 9.3 kHz. The frequency stability obtained using this optical package in a bench setup was $4 \times 10^{-11} \tau^{1/2}$ in the range $1 \text{ s} < \tau < 30 \text{ s}$. The frequency stability degraded to about 10^{-10} at an averaging time of 1000 s, caused by a rather important linear frequency drift of -5×10^{-9} per day. Similar results were obtained with Cs. Other work made towards the implementation of small cells has been reported [33, 34].

Other studies have been initiated using amplitude modulation of the laser to generate the field required to create the CPT phenomenon [83]. The goal is to use very high buffer-gas pressures to inhibit diffusion to the cell walls and thus making possible narrow resonance lines in very small cells. The idea is based on the concept that CPT behaves differently when amplitude modulation of the laser is used instead of frequency modulation to create the sidebands. With amplitude modulation, it appears that the excitation of the CPT phenomenon is possible with broad overlapping optical lines (large buffer-gas pressures) [84]. In the case of frequency modulation, the observation of the CPT signal requires that the optical lines be resolved, making the signal amplitude a function of the buffer-gas pressure.

In order to increase signal to noise ratio, other techniques have been proposed, of which some have been mentioned above. One consists in using so-called end transitions, with the advantage of weaker spin-exchange relaxation and an increase in signal amplitude [85, 86]. However, these end transitions are field dependent in first order, a property that adds a difficulty in the practical implementation of a frequency standard. So-called push–pull optical pumping, in which the light polarization is alternated between right and left circular polarization, has been proposed to enhance the 0–0 transition [65]. The lin-per-lin polarization approach, having a similar property, has been mentioned above [68]. Another technique using a so-called ‘polarization-selective method’ for enhancing the signal amplitude without increasing light shift has also been studied [87]. Finally, a technique has been proposed in which circularly polarized σ^+ radiation is retro-reflected after traversing the resonance cell providing a σ^- radiation beam [66, 67]. In that case the ensemble is submitted to a double Λ scheme and the signal in principle is enhanced.

4.2.5 Discussion of frequency stability. The expected frequency stability may be calculated with Eq. (44) in the limit of shot noise. The quality figure q is obtained from the contrast and the line width as calculated above. In Ref. [27], for a temperature of the order of $65\text{--}70^\circ\text{C}$, a q figure of the order of 1.5×10^{-4} for a background intensity $I_{\text{bg}} = 10 \times 10^{-6} \text{ A}$ is obtained. The resulting expected calculated frequency stability is of the order of $7 \times 10^{-14} \tau^{-1/2}$.

Unfortunately, such frequency stability is not observed experimentally, as shown above. A frequency stability of the order of $3\text{--}5 \times 10^{-11} \tau^{-1/2}$ has been a common observation in most devices, two orders of magnitude less than that expected from the limit of shot noise [27, 61, 79, 82]. It should also be mentioned that this behavior is also reported in the case of the classical passive IOP frequency standard using a solid-state diode laser as the optical pumping source [88, 89].

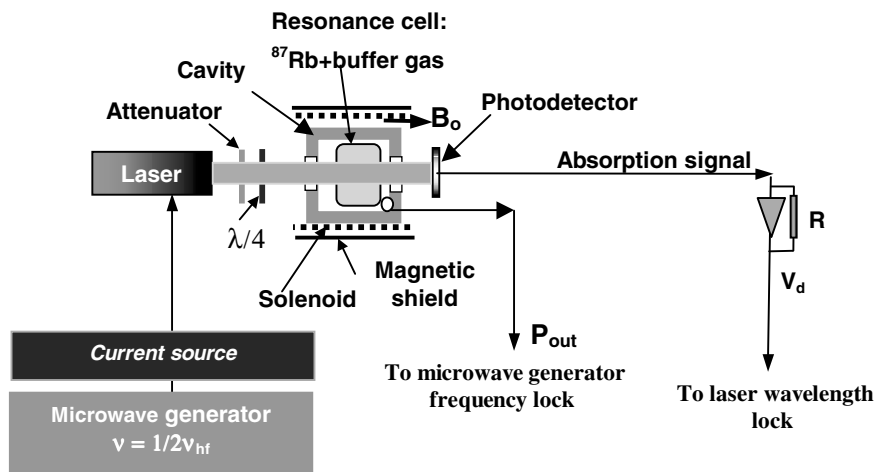


FIGURE 14 Block diagram of the CPT maser using ^{87}Rb

It is believed that this behavior is due to the inherent AM and FM noise imbedded in the laser radiation. The AM noise appears directly at the photodetector as intensity noise and adds directly to shot noise. This noise contributes to the order of several parts in 10^{-13} to the frequency instability and of course depends on the relative intensity noise (RIN) of the laser used. On the other hand, it is believed that the laser FM noise is converted into AM fluctuations by the nonlinear optical resonance absorption within the ensemble [63, 64]. It also adds directly to shot noise at the detector. Experiments have been made in order to compensate this effect by either reducing the spectral width of the laser spectrum or by direct compensation by means of a clone resonance cell in the IOP approach [89]. Relative success was obtained in the latter case and, although the technique is somewhat complex, it appears to provide an avenue for reducing the effect.

5 The active approach in a cell: the CPT maser

Another approach using CPT for implementing a frequency standard consists in exploiting directly the hyperfine coherence created in the ground state as in a maser. This coherence creates in turn an oscillating magnetization at the same frequency [26, 29]. When the ensemble is placed in a cavity the magnetization excites the cavity mode and creates an oscillating magnetic field. This oscillating magnetic field reacts back on the atomic ensemble and causes stimulated emission in the same manner as in a maser. This CPT maser has very interesting characteristics such as absence of thresholds relative to pumping rate, alkali-atom density, and cavity Q , a great improvement over the intensity-pumped Rb maser which has critical threshold conditions relative to these parameters [90]. It may be mentioned that these threshold conditions have prevented the practical realization of a Cs maser using IOP [91], while the same Cs maser was readily implemented using CPT [26]. A block diagram of a typical implementation of a CPT ^{87}Rb maser is shown in Fig. 14.

The analysis of the CPT maser is more complex than that of the passive approach, in view of the interaction of the atoms with the microwave field in the cavity. The analysis must take

into account the phase relationship ϕ between the microwave field and the oscillating magnetization. Furthermore, the phase of the optical fields is coupled to the hyperfine coherence. An analysis taking into account the interrelation between these phases has been developed in the case of a closed three-level system [92]. A more exact analysis of the CPT maser characteristics including optical pumping in an open system is more complex. However, the most important characteristics of the maser may be obtained from approximate models that provide some insight into the physical phenomena taking place. For this reason, we will outline a few approaches that make explicit the fundamental characteristics of the maser under specific conditions of operation as a frequency standard.

5.1 Basic maser theory

The experimental setup used in the analysis is that illustrated in Fig. 14 with the cavity tuned close to the hyperfine frequency. In a maser, the energy given by the atomic ensemble is dissipated in the cavity walls and coupling loop. The analysis using this so-called self-consistent approach is given in Annex C. It is shown that the power delivered by the atoms is given by

$$P_{\text{at}} = \frac{1}{2} \frac{N\hbar\omega k}{(1 + 4Q_L^2(\Delta\omega_c/\omega_{\mu'\mu})^2)} |2\delta_{\mu'\mu}|^2, \quad (52)$$

where N is the total number of alkali atoms, k is the gain factor, Q_L is the cavity loaded quality factor, and $\Delta\omega_c$ is the cavity detuning relative to the atomic resonance angular frequency $\omega_{\mu'\mu}$. An important relation is also obtained between the Rabi frequency b , a measure of the microwave field intensity in the cavity, and the coherence $\delta_{\mu'\mu}$ existing in the ensemble:

$$\langle b \rangle = 2k|\delta_{\mu'\mu}|, \quad (53)$$

where the brackets $\langle \rangle$ mean average over the length of the resonance cell and the double bars $||$ mean absolute value. On the other hand, the phase between the field and the magnetization in the ensemble is given by

$$\phi = \frac{\pi}{2} + \tan^{-1} 2Q_L \frac{\Delta\omega_c}{\omega} - \tan^{-1} \frac{\delta_{\mu'\mu}^i}{\delta_{\mu'\mu}^r}, \quad (54)$$

making explicit the phase quadrature, close to $\pi/2$, between these two physical quantities. The problem is thus one of evaluating the coherence $\delta_{\mu'\mu}$. This is done from the rate equations. Several approximations adapted to the experimental situation at hand can be made in such a process and they are outlined in the following paragraphs.

5.2 Homogeneous model

A simple approach for obtaining an expression for the maser power output consists in assuming that the ensemble is optically thin and in replacing $\delta_{\mu'\mu}$ in Eq. (52) by the value found in Eq. (40). This approximation is valid only at low temperatures. In doing so, one neglects entirely the feedback of the microwave field on the atomic ensemble coherence and on the population of the levels. This is actually rather approximate, but the exercise provides nevertheless some insight into the behavior of the maser. In that exercise, it is readily observed that the maser does not have a threshold relative to cavity Q , density, line width, or pumping rate.

A more realistic model consists in solving the set of rate equations (11)–(16) with the presence of the microwave Rabi frequency in the equations and taking into account its coupling to the coherence by means of Eq. (53). The system may then be solved taking into account the phase of the microwave radiation given by Eq. (54). The results show again that the maser does not have a threshold relative to the parameters mentioned above [92].

5.3 Inhomogeneous model

In practice, however, as in the case of the passive approach, the system becomes optically thick at normal temperatures of operation and the ensemble cannot be considered homogeneous. In such a case, the amplitudes of the various parameters vary along the length of the cell and the set of equations (11)–(16) is valid only locally, that is for a thin slice of the medium. Furthermore, the phase of the laser sidebands is coupled to the microwave field and varies along the length of the cell. The problem has been solved in the case of a closed three-level system by dividing the cell into small slices and by means of a numerical integration over the cell length of the Rabi frequency b , which is a function of distance and sidebands' phase [93].

It is found in particular that the calculated maser power is a function of the ratio of cell length to microwave wavelength. In fact, for low densities, and a cell whose length L is equal to $\lambda_{\mu w}$, the power output is equal to zero. This effect results from the fact that the elementary magnetizations in each slice emit with their own phase. The phase of the microwave radiation created in the second half of the ensemble is opposite to that of the radiation created in the first half. However, at high densities, the system is not homogeneous and the phase cancelation from one part of the cavity to the other is not exact: the part of the cell at the entrance of the cavity contributes more than the part at the exit of the cavity since radiation is strongly absorbed. Nevertheless, the power calculated still decreases for cell lengths larger than $\sim \lambda/2$.

The analysis can also be developed for the four-level model developed above in the case of the passive approach. In that case, in order to simplify the analysis, the cell dimension is assumed less than a half wavelength and the variation of phase is neglected along the length of the cell. The solution consists in dividing the cell into thin slices and solving Eqs. (11)–(16) for each of these slices, as was done in the case of the three-level model. The value of the Rabi frequency is calculated at each slice by means of Eq. (37) with α defined by Eq. (38) as in the case of the passive approach. The problem is reduced to one of solving the resulting set of equations that includes the self-consistent condition in which the power emitted by the ensemble is equal to that lost in the cavity. Those equations are

$$b = -2\frac{k}{L} \int_0^L \delta_{\mu\mu'}^r(z) dz, \quad (55)$$

$$\frac{\partial}{\partial z} \Gamma_p = -\alpha \frac{2\Gamma_p}{3\Gamma^*} \left\{ 1 - \frac{(2/3)\Gamma_p/\gamma_1}{1 + (2/3)\Gamma_p/\gamma_1} + 3\delta_{\mu\mu'}^r \right\}, \quad (56)$$

$$\left(\gamma_1 + 2\Gamma_p + \frac{b^2}{\gamma_1 + 2\Gamma_p} \right) \delta_{\mu\mu'}^r = -\Gamma_p \left\{ \frac{2/3}{1 + (2/3)\Gamma_p/\gamma_1} \right\}, \quad (57)$$

where the pumping rate is given by

$$\Gamma_p = \frac{\omega_R^2}{2\Gamma^*}. \quad (58)$$

The power emitted by the atomic ensemble is given by

$$P_{\text{at}} = \frac{kN_a}{2L^2} \hbar\omega_{12} \left[2 \int_0^L \delta_{\mu\mu'}^r(z) dz \right]^2. \quad (59)$$

These equations are solved through a recursive method in which the Rabi frequency b is first given a value. Integration is then done numerically for a given value of the pumping rate Γ_p at the entrance of the cell. The solution provides a new value of b , which is then assumed as the initial parameter for a new integration. The process converges rapidly. The result of this exercise is shown as the solid lines in Fig. 15 as a function of the pumping rate Γ_p for three values of α corresponding to the temperatures indicated. Experimental results obtained in similar conditions are shown as points on the same graph [77]. It should be pointed out that in general the density of atoms in the Rb ensemble is not well known and depends to a large extent on the previous temperature cycling of the cell used or its history [94, 90]. The experimental value of the density is usually smaller than that obtained from tables. For this reason, the free parameter used in the adjustment of the theoretical results to the experimental data is the power output, a function of density. It has been adjusted to match approximately the maser power at the highest temperature. It is observed that this procedure provides nevertheless a qualitative agreement with the experimental data.

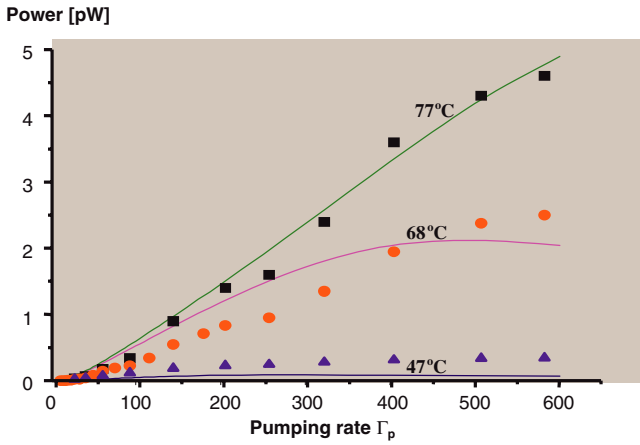


FIGURE 15 Power output of the CPT ^{87}Rb maser. Continuous solid lines are obtained from the four-level model developed in the text while the points are experimental [77]

5.4 Frequency stability

The CPT maser may be considered as a hybrid device, the atoms emitting energy, but at a frequency given by the difference of the two laser sidebands, $\omega_1 - \omega_2$. In that case, the frequency of the microwave generator used to modulate the laser needs to be locked to the frequency of the maser emission line maximum by synchronous detection, as in the passive case. It is thus a frequency-lock system similar to that used in the case of a passive maser. Considering only thermal noise, the short term frequency stability limit of the CPT maser may be written as [77, 95]

$$\sigma(\tau) \approx \sqrt{\frac{F k_B T}{P_o} \frac{1}{Q_a} \tau^{-1/2}}, \quad (60)$$

where T is the temperature of the cell-cavity arrangement, P_o is the power output of the maser, Q_a is the atomic line quality factor, and F is the noise figure of the amplifier in the first stage of the receiver. Since the output frequency is the difference frequency of the correlated sidebands, laser frequency noise should not affect the CPT maser output frequency directly. However, these fluctuations may affect the maser frequency stability through the light shift that will be examined below. As in the case of the passive CPT approach it is important to minimize the maser line width to obtain the largest possible line Q in order to maximize frequency stability. Similarly, higher emission power improves frequency stability. However, since higher power generally leads to a greater line width, a trade off must be made. In a typical situation, around 60°C with a pumping rate of 300 s^{-1} , the power delivered by the atoms to the cavity is typically $1 \times 10^{-12}\text{ W}$. The line width is of the order of 175 Hz providing a line Q_a of 3.9×10^7 . With a receiver noise figure of 1.2, the expected frequency stability is then of the order of $2 \times 10^{-12} \tau^{-1/2}$. An experimental setup in which a crystal oscillator was frequency locked to the maser power output maximum gave, under conditions similar to those just described, a short-term frequency stability of the order of $3 \times 10^{-12} \tau^{-1/2}$ [95]. The implementation was not optimized and a better frequency stability could

be realized through the use of a better quartz-crystal oscillator in the frequency-lock loop [77].

5.5 Frequency shifts

All the shifts mentioned in the case of the CPT passive frequency standard approach are present in the CPT maser. Furthermore, there are frequency shifts that are particular to the maser.

In particular, a detuning of the laser by Δ_o coupled to a difference in amplitude of the laser sidebands produces a frequency shift given by

$$\Delta\omega_{\text{LS}} = -\frac{(1 - \beta^2)\omega_{\text{R1}}^2}{4} \left\{ \frac{\Delta_o}{(\Gamma^*/2)^2 + \Delta_o^2} \right\}, \quad (61)$$

where β is the ratio of the sidebands' amplitudes. This is totally different from the case of the passive CPT standard where such a condition, laser detuning and difference in sidebands, produces a distortion of the resonance line without displacement of its maximum. This is due to the fact that, in the two approaches, different physical observables are measured. In the case of the passive approach, the optical coherence is the measured parameter through the absorption of the medium, while in the case of the maser it is the ground-state coherence that is detected and measured directly.

On the other hand, the interaction of the atomic ensemble with the cavity microwave field creates added frequency shifts such as the cavity pulling, a microwave power shift, and a propagation shift.

The cavity pulling is well known and is common to all masers. In the case of the CPT maser, which is a hybrid between an oscillating maser and a passive maser, the shift is a function of the importance of the microwave feedback on the atomic ensemble. The effect can be evaluated analytically in the case of the homogeneous model. Cavity detuning from hyperfine resonance introduces a phase shift between the field and the magnetization given by the second term of Eq. (54). This phase shift produces a maser frequency shift given by

$$\Delta\nu = \frac{Q_L}{Q_a} \Delta\nu_c (S - 1), \quad (62)$$

where Q_L is the cavity loaded Q , Q_a is the atomic line Q , $\Delta\nu_c$ is the cavity detuning, and S is the ratio of the total line width including microwave interaction (power-broadened line width) to the line width including all causes except the microwave interaction (natural line width). The natural line width is that calculated by means of Eq. (43) with the optical Rabi frequency ω_R homogeneous along the cell. The power-broadened line width is the natural line width, with the addition of the saturation factor, $b^2/(\gamma_1 + 2\Gamma_p)$. In this homogeneous model, the shift creates a stringent demand on the frequency stability of the cavity resonance frequency. For a cavity Q_L of 10 000, and a line Q_a of 5×10^7 , the cavity must be stable to within 3 to 4 Hz to obtain a maser fractional frequency stability of the order of $\sim 10^{-13}$. In the inhomogeneous case where the parameters vary along the cell length, a numerical calculation shows that the effect is somewhat reduced [77].

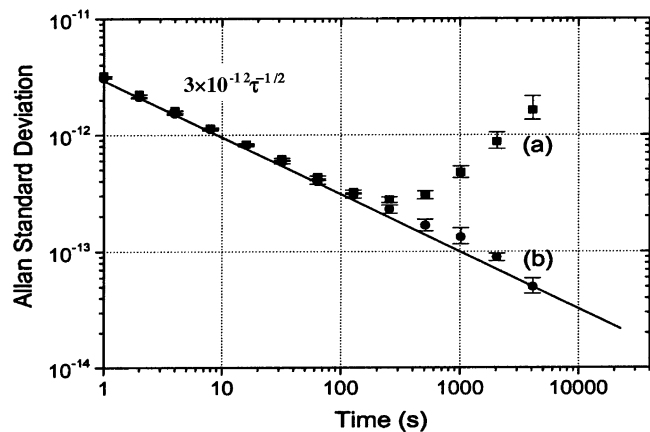


FIGURE 16 Frequency stability observed in a CPT ^{87}Rb maser: (a) full data; (b) drift removed (from [95])

The microwave power shift originates from the fact that upon stimulated microwave emission the populations of the ground levels are no longer equal. This creates an asymmetry in the system and an effect similar to the linear light shift mentioned above (Eq. (61)) is introduced. It adds directly to the light shift calculated previously for the effect of sidebands of different amplitudes.

Finally, an important effect predicted by the analysis is the introduction of a frequency shift associated with the phase of the sidebands' radiation. The shift has been called a propagation shift and becomes rather important in the case of high densities [77]. It has the effect of altering the value of the modulation index for which the power light shift becomes zero. It can thus be canceled in the same way as the sideband light shift by a proper adjustment of the modulation index [77, 95]. Figure 16 is an illustration of the frequency stability that has been measured for a CPT ^{87}Rb maser [95].

It is possible that in the setup studied, the behavior of the frequency stability observed for $\tau > \sim 200$ s is due to fluctuations of the frequency shifts discussed above. It should be mentioned that in the particular setup reported, the maser cavity was made of copper with a temperature sensitivity of more than 100 kHz per degree and operated at atmospheric pressure [96]. In that case, environmental fluctuations may have a direct effect on the cavity tuning and cause long-term random fluctuations or frequency drifts that will be reflected by an increasing $\sigma(\tau)$ such as the one observed.

6 CPT in laser-cooled ensemble and pulsed approach

In the approaches reviewed above, first-order Doppler broadening of the hyperfine resonance line is avoided either by using a buffer gas (Dicke effect [48]) or by using the separated interaction zone technique (Ramsey separated field approach [23]). However, as was readily seen, these techniques have limitations.

In the case of the buffer-gas technique, a large frequency shift as well as a temperature dependence is introduced. Furthermore, in the approach described above, although substantial narrowing is introduced even in cells of small dimensions, broadening of the resonance line proportional to the

light intensity is always present. It is possible to use low light intensity but this can only be done at the expense of signal size. In the case of the atomic beam approach, the system is sensitive to various parameters such as the phase shifts and the relative orientations of the laser beams and of the atomic beam.

A proposal has been made to address these problems by avoiding altogether the use of buffer gases and atomic beams. The approach uses the so-called isotropic cooling technique [97–99]. An ensemble of the order of 10^8 Cs atoms has been successfully cooled in a cell to a temperature of a few μK . However, since the process of cooling requires intense laser radiation, it follows that the ensemble is strongly perturbed by the process. For this reason, it is proposed to use a pulse approach in both the cooling and the resonance interaction with the atoms in the implementation of the resulting frequency standard. There are several ways of extracting the actual resonance information, as for example using a probe laser to measure the cell transparency under excitation by means of a microwave field as in the classical IOP double-resonance approach. A possible variant of this approach consists in using the Ramsey separated field technique but in the time domain rather than in space. This Ramsey time-domain approach in a cell had been examined originally in the 1960s using a double-resonance, microwave-spectral lamp, approach [100]. It has been revisited more recently using laser optical pumping [101]. It is thus expected that the same technique applied to an ensemble of cold atoms should provide similar promising results. In fact, preliminary results obtained on an ensemble of cooled atoms, using a microwave cavity and the double-pulse optical-microwave excitation technique, showed a Ramsey central fringe having a width of ~ 14 Hz [102]. In practice, due to free fall in the Earth's gravitational field, it appears that the width of such fringes will be limited to about 10 Hz.

However, the technique just described requires a microwave structure in order to excite transitions. The CPT approach, on the other hand, can be used without this microwave structure and two avenues are possible. In the first avenue, a single laser pulse, consisting of two radiation fields at frequencies ω_1 and ω_2 as illustrated in Fig. 1b, is applied after the cooling pulse. It has the advantage of simplicity and the CPT resonance phenomenon can then be detected either in transmission or in fluorescence [32]. The approach, however, has the disadvantage of line broadening by the laser pulse exciting the CPT resonance.

In a second avenue, it is proposed to use CPT pulses, implementing the Ramsey separated interaction zones technique as in the Thomas et al. approach described above [22], but in the time domain rather than in the space domain. Preliminary experiments towards the use of this approach have been made in a cell containing a buffer gas [103]. The analysis done by Zanon [103] using a wave-function approach is similar to that outlined above in the case of CPT applied to an atomic beam. However, relaxation, due to buffer-gas collisions, spin-exchange interaction, and diffusion taking place while the ensemble evolves freely between the laser pulses, must be included in the analysis. The results of the analysis are in agreement with the experimental data [68, 103]. A line width of about 60 Hz was obtained for the Cs central

Ramsey fringe in a cell containing a nitrogen buffer gas at a pressure of 23 Torr and pulses separated by 8 ms. These preliminary experiments provide a proof of concept for the use of the time-domain CPT Ramsey-technique approach in an isotropically cooled ensemble.

7 Conclusion

In this paper, we have reviewed developments made up to now on the use of the coherent population trapping phenomenon as applied to the implementation of frequency standards. The review was made for several approaches either in the continuous or pulsed mode or for closed cells and atomic beams. It may be concluded that CPT offers in general considerable advantages over the classical approaches using either intensity optical pumping or magnetic state selection regarding certain characteristics of the implemented frequency standards.

The approach using CPT with an atomic beam has been studied in some detail. Experimental results making explicit the presence of frequency shifts, such as those caused by the ac Stark effect and misalignment of laser beams and the atomic beam, have been reported. Although they appear to be important, they are well understood, and a frequency stability in agreement with that calculated on the basis of limiting shot noise in the detection system has been realized in laboratory implementations. Although the approach offers some rather interesting characteristics, it does not appear to be pursued at this time in either national institutions or private establishments.

The passive approach in a sealed-off cell allows simplicity in construction and makes possible the realization of relatively small frequency standards with a frequency stability similar to that obtained in small units using the classical double resonance intensity optical pumping approach ($3 \times 10^{-11} \tau^{-1/2}$). The CPT technique is also adaptable to the realization of very small optical packages (cells $\sim \text{mm}^3$), but at the expense of a larger line width, a smaller signal or contrast, and consequently lower frequency stability. Several laboratories are active in the development of such a passive standard, and research is carried out in several institutions in order to understand better the physics involved and to develop techniques that will improve signal amplitude without broadening the resonance line.

The maser approach in a sealed-off cell also provides a certain advantage over techniques of similar nature. Its implementation is simplified by the absence of oscillation thresholds and a short-term frequency stability of the order $3 \times 10^{-12} \tau^{-1/2}$ has been measured. The approach appears to offer intermediate short-term stability between the passive Cs–Rb frequency standards and the H maser, in a relatively small unit that could find use in some critical applications. Development is being carried out in some national laboratories [104] and in industry [105].

Finally, an approach using pulsed CPT for implementing a laser-cooled frequency standard in a cell shows promise relative to frequency stability and size and is under study at one institution [106].

It may finally be concluded that coherent population trapping provides a new, fresh, breeze in the practical imple-

mentation of field-operable atomic frequency standards in the microwave range. A sustained effort should lead in the not too distant future to the realization of frequency standards that will fulfill specific needs regarding frequency stability and size and add to the pool of available classical atomic frequency standards.

Annex A. Derivation of the expressions for the Ramsey fringes and phase in the CPT beam approach

In this annex, we outline the calculation of the expression for the Ramsey fringes and their phase in the case of the CPT beam approach. We use an operator formalism [21] somewhat different from that used by Hemmer et al. [53]. In reference to Fig. 1b, we define the following terms:

$$\delta_o = \frac{2\Delta_o}{\Gamma}, \quad (\text{A1})$$

$$\xi = \frac{\Omega_R^2/\Gamma^2}{1 + \delta_o^2}, \quad (\text{A2})$$

$$\Omega_\mu = \omega_{12} - \omega_{\mu\mu}. \quad (\text{A3})$$

We apply the adiabatic approximation to the evolution of the excited state. In that case, it is assumed that the excited-state response is so rapid that it follows the evolution of the ground state and is essentially in stationary equilibrium at all times. The set of equations (11)–(16) is then reduced to three equations containing only ground-state matrix elements and atomic parameters. We obtain

$$\delta_{\mu\mu'}^r = -\frac{\Gamma\xi}{1 + 3\xi}\delta_{\mu\mu'}^r - \frac{1}{2}\frac{\Gamma\xi}{1 + 3\xi} + \Omega_\mu\delta_{\mu\mu'}^i, \quad (\text{A4})$$

$$\delta_{\mu\mu'}^i = -\Gamma\xi\delta_{\mu\mu'}^i + \frac{1}{2}\Gamma\xi\delta_o(\rho_{\mu\mu} - \rho_{\mu'\mu'}) - \Omega_\mu\delta_{\mu\mu'}^r, \quad (\text{A5})$$

$$\frac{d}{dt}(\rho_{\mu\mu} - \rho_{\mu'\mu'}) = -\Gamma\xi(\rho_{\mu\mu} - \rho_{\mu'\mu'}) - 2\Gamma\xi\delta_o\delta_{\mu\mu'}^i. \quad (\text{A6})$$

The fluorescence power in zone B is given by

$$P_{\text{fl}} = \int \hbar\omega N\Gamma\rho_{\text{mm}} dt \quad (\text{integral over zone B}) \quad (\text{A7})$$

and the population of the excited state ρ_{mm} is given by

$$\rho_{\text{mm}} = \frac{\xi}{1 + 3\xi}(1 + 2\delta_{\mu\mu'}^r). \quad (\text{A8})$$

The set of equations (A4)–(A6) can be written in matrix form as

$$\begin{aligned} & d/dt \begin{pmatrix} \delta^r \\ \delta^i \\ \rho_{\mu\mu} - \rho_{\mu'\mu'} \end{pmatrix} \\ &= \begin{pmatrix} \xi\Gamma/(1 + 3\xi) & \Omega_\mu & 0 \\ -\Omega_\mu & -\Gamma\xi & (1/2)\Gamma\xi\delta_o \\ 0 & -2\Gamma\xi\delta_o & -\Gamma\xi \end{pmatrix} \\ &\times \begin{pmatrix} \delta^r \\ \delta^i \\ \rho_{\mu\mu} - \rho_{\mu'\mu'} \end{pmatrix} + \begin{pmatrix} -\xi\Gamma/2(1 + 3\xi) \\ 0 \\ 0 \end{pmatrix}. \quad (\text{A9}) \end{aligned}$$

We may then represent the state of the ensemble as the vector v :

$$v = \{\delta^f, \delta^i, \rho_{\mu\mu} - \rho_{\mu'\mu'}\}. \quad (\text{A10})$$

The effect of CPT in the interaction zones is obtained by solving Eq. (A9). It may be represented by a pseudo-rotating operator $M_i(\Omega_R, \Omega_\mu \delta_o, t)$, $i = A, B$, or C , affecting state vector (A10) [21]. In zones A and B, M is obtained from Eq. (A9) by means of Laplace transformation and has the form

$$M(\Omega_R, \Omega_\mu, \delta_o, t) = \begin{pmatrix} \exp\left(-\frac{t\Gamma\xi}{1+3\xi}\right) & 0 & 0 \\ 0 & \exp(-t\Gamma\xi) \times \cos[t\Gamma\xi\delta_o] & \frac{1}{2}\exp(-t\Gamma\xi) \times \sin[t\Gamma\xi\delta_o] \\ 0 & 2\exp(-t\Gamma\xi) \times \sin[t\Gamma\xi\delta_o] & \exp(-t\Gamma\xi) \times \cos[t\Gamma\xi\delta_o] \end{pmatrix}. \quad (\text{A11})$$

In the operation, however, a term appears that is not coupled to the components of v_o . It is not included in $M(\Omega_R, \Omega_\mu, \delta_o, t)$ and is thus introduced as a vector v_s :

$$v_s = \left\{ (1/2) \left(-1 + \exp\left[-\frac{\Gamma\xi t}{1+3\xi}\right] \right), 0, 0 \right\}. \quad (\text{A12})$$

This vector must be added to the state vector resulting from the transformation of v_o by $M(\Omega_R, \Omega_\mu, \delta_o, t)$. At the exit of zone A the state vector is thus

$$v_A = M_A \bullet v_o + v_s. \quad (\text{A13})$$

In zone C where the atoms evolve freely, the operator has the form

$$M(0, \Omega_\mu, 0, t) = \begin{pmatrix} \cos t\Omega_\mu & \sin t\Omega_\mu & 0 \\ -\sin t\Omega_\mu & \cos t\Omega_\mu & 1 \\ 0 & 0 & 0 \end{pmatrix}. \quad (\text{A14})$$

The final state vector in zone B is obtained by successive transformation applied to the resulting state vector v , taking into account the remark made in connection with v_s in zones A and B.

In the calculation, we have assumed that in zones A and B the intensity of the laser radiation is very large and that the CPT resonance line is broadened to the extent that the small detuning Ω_μ is negligible. We call ϕ_A the phase of the coherence at the exit of the first zone, defined through the relation

$$\delta_{\mu\mu'} = |\delta_{\mu\mu'}| e^{i\phi_A}. \quad (\text{A15})$$

After performing the operation of Eq. (A13), we obtain $\delta_{\mu\mu'}$ at the exit of zone A, and the phase is given by

$$\tan[\phi_A] = \frac{\alpha^i}{\alpha^f} = \frac{\exp[-\Gamma\xi\tau_A](\rho_{\mu'\mu'} - \rho_{\mu\mu})_o \sin[\Gamma\xi\delta_o\tau_A]}{1 - \exp\left[-\frac{\Gamma\xi\tau_A}{1+3\xi}\right]}. \quad (\text{A16})$$

Finally, after successive application of operator M in each zone, the fluorescence integrated over zone B is calculated as

$$P_{\text{fl}}(\text{zone B}) = (1 - \exp[-\Gamma\xi\tau_B/(1+3\xi)]) \times N\hbar\omega\{1 + (-1 + \exp[-\Gamma\xi\tau_A/(1+3\xi)]) \times |\sec[\phi_A]|\cos[\phi_A - T\Omega_\mu]\}. \quad (\text{A17})$$

Equations (A16) and (A17) are the expressions used in the main text¹.

Annex B. Optical absorption of polarized laser radiation including optical pumping

This annex concerns optical absorption spectra of the cell used in the CPT passive approach experiments described in this paper. The level structure of the lower manifold of ⁸⁷Rb pertinent to the present discussion is shown in Fig. B1.

The absorption spectra under various conditions are shown in Fig. B2. The spectra are obtained for two light intensities and two polarizations, linear polarization propagating in the direction of the magnetic field, called σ , and circular polarization, σ^+ (or σ^-). As is clearly observed in that figure, there is a drastic change in behavior in passing from linear polarization to circular polarization. Absorption through transition ‘a’ is considerably reduced under circular polarization. The transition probabilities between the various Zeeman sublevels cannot alone explain this behavior. In fact, a summation over all these levels considering appropriate transitions gives equal transition probabilities whatever the polarization. The effect can only be explained through a detailed examination of the dynamics of the transitions causing optical pumping that takes place in the presence of a buffer gas. This is shown in Fig. B3 for the case of σ^+ polarization. As is observed, for transition ‘a’, levels $F = 2$, $m_F = 1$ and 2 are not connected by the radiation. For transition ‘b’, only level $F = 1$ and $m_F = 2$ is not connected. Atoms excited to the P state decay to all levels equally due to collisions with the buffer gas and are trapped in these levels. This effect is essentially an optical pumping process [10]. Decay from the excited state takes place at rate Γ^* ($\sim 10^9 \text{ s}^{-1}$), while equilibrium in the ground state is re-established through relaxation at rate γ_1 ($\sim 10^3 \text{ s}^{-1}$). There are thus a large number of atoms trapped in these levels and they no longer contribute to absorption.

The situation for transitions ‘c’ and ‘d’ originating from level $F = 1$ is different, as is seen in Fig. B3. Only level $F = 1$ and $m_F = 1$ can act as a trap for transition ‘c’. However, in all

¹It is noted that the expression given by Hemmer et al. [53] for the phase shift is different from ours by a factor of two in the argument of the ‘sin’ term. The appropriate expression obtained from Eq. (8) using their notation is.

$$\tan[\phi_A] = \frac{-\exp[-\Omega^2 S \tau_A](\rho_{\mu'\mu'} - \rho_{\mu\mu})_o \sin[2\Omega^2 D \tau_A]}{\exp[-f \Omega^2 S \tau_A] - 1}, \quad (\text{A18})$$

where the various terms are connected to those used in the present paper by the relations

$$\Gamma\xi = \Omega^2 S, \quad (\text{A19})$$

$$\Gamma\xi/(1+3\xi) = f \Omega^2 S, \quad (\text{A20})$$

$$\Gamma\xi\delta_o = 2\Omega^2 D. \quad (\text{A21})$$

An analysis by Shahriar et al. made later [107] is compatible with this conclusion.

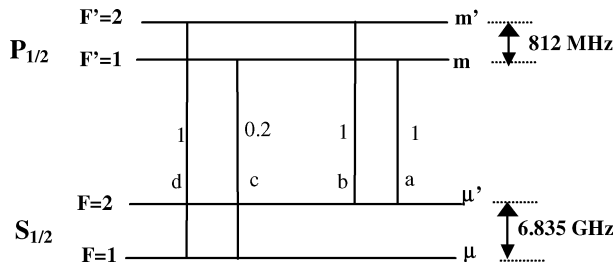


FIGURE B1 Lower levels $P_{1/2}$ and $S_{1/2}$ of the ^{87}Rb atom. The numbers beside the vertical lines are transition probabilities summed over the Zeeman sublevels of each manifold

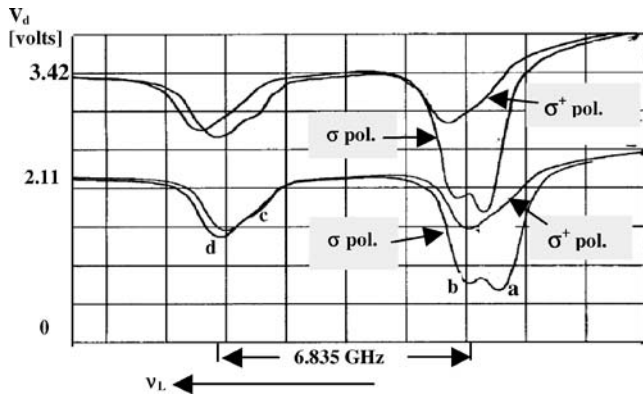


FIGURE B2 Absorption spectrum of a ^{87}Rb cell under linear polarization (σ) and circular polarization (σ^+). The laser is not modulated. The absorption lines are identified by 'a', 'b', 'c', and 'd' corresponding to the transitions shown in Fig. B1. The absorption spectrum is shown for two light intensities of 21 μW (2.11 V) and 34 μW (3.42 V) incident on the cell

cases the other hyperfine level not involved in the transition can also act as a trap. The only difference between the two cases is related to the number of trapping levels involved. In the case of σ polarization the situation is radically different. A similar representation as that shown in Fig. B3 shows that transitions are possible from all Zeeman sublevels and there are no trapping levels as in the previous case. Optical pumping is possible only to the other hyperfine level not involved in the transition.

An analysis can be made of this effect using the tools developed in the present paper. Since there is only one radiation field present there is no coherence introduced in the ground state. Solving Eq. (37) through numerical integration, we can calculate readily the intensity of the transmitted radiation (square of the amplitude of the optical Rabi frequency) at the exit of the cell. The required expression of the optical coherence is calculated from rate equations similar to the set (11)–(16). In the calculation we assume the appropriate number of trap levels as determined from Fig. B3 for σ^+ polarization, and from a similar one for σ polarization. We use tabulated values of transition probabilities. This is done for two intensities approximating the experimental situation shown in Fig. B2. The result of this exercise is shown in Fig. B4.

These results can be compared to the actual absorption spectrum of laser radiation shown in Fig. B2. It appears that the model developed based on optical pumping explains rather well at least qualitatively the experimental observations. The net effect is a transfer of population from absorbing levels to other levels not coupled by the radiation, decreasing consider-

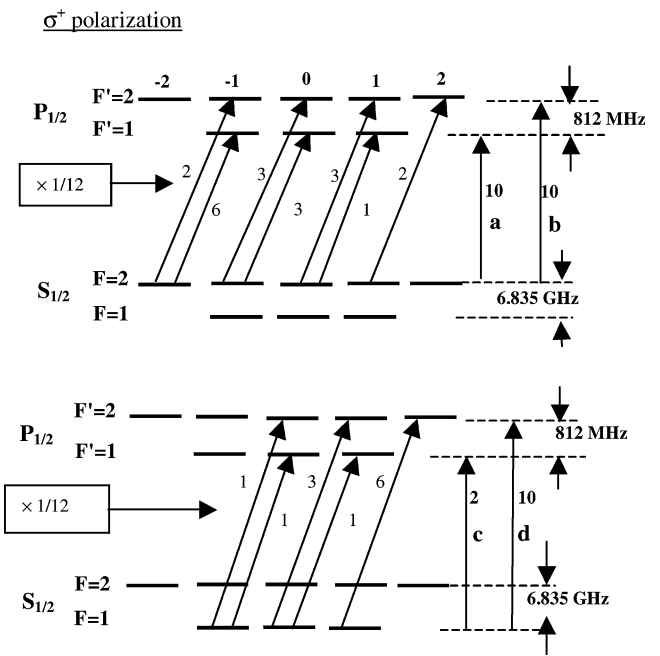


FIGURE B3 Manifold of ^{87}Rb lower energy levels used to illustrate the characteristics of optical absorption. The numbers attached to the arrows are transition probabilities

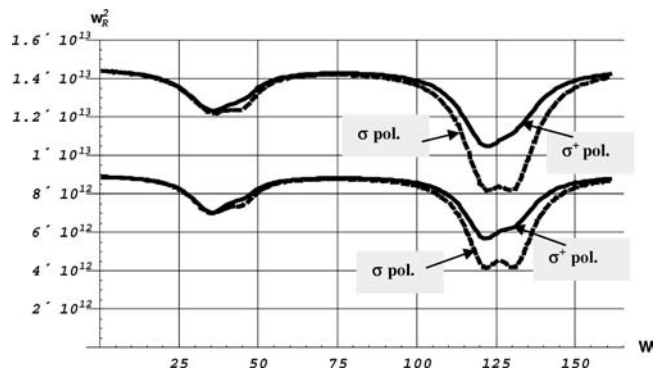


FIGURE B4 Calculated absorption spectrum (D1) by a cell containing ^{87}Rb and a buffer gas for two values of the intensity of monochromatic laser radiation corresponding approximately to those used in the case of Fig. B2. The constants assumed in the calculation are $\alpha = 2.1 \times 10^{11} \text{ m}^{-1} \text{ s}^{-1}$ and $\Gamma^* = 2 \times 10^9 \text{ s}^{-1}$

ably the absorption and affecting the shape of the overlapping absorption lines. The present results validate to a certain extent the four-level model that was used in the calculation outlined above in connection with the CPT hyperfine resonance transmission contrast and the maser power output.

Annex C. Basic CPT maser theory

In a maser, the energy given by the atomic ensemble is dissipated in the cavity walls and coupling loop. In a self-consistent approach, for continuous oscillation, it is required that the power emitted by the atoms equals the power dissipated in the cavity. The power dissipated in the cavity of volume V_c is given by [108]

$$P_{\text{cav}} = \frac{\mu_0 \omega}{2Q_L} \int_{V_c} |H(r)|^2 dV, \quad (\text{C1})$$

where Q_L is the loaded quality factor of the cavity, μ_0 is the permeability of free space, and ω is the angular frequency of the oscillating magnetic field $H(r)$ in that cavity. Using Eq. (5), this expression can be written in terms of the Rabi angular frequency b as

$$P_{\text{diss}} = \frac{1}{2} \frac{N\hbar\omega}{k} \mu_0 \langle b \rangle_{\text{bulb}}^2, \quad (\text{C2})$$

where the brackets $\langle \rangle_{\text{bulb}}$ mean an average over the length of the bulb (resonance cell) containing the ensemble of alkali atoms N . The gain parameter k , in units of photons per atoms per second, is defined as

$$k = \frac{N Q_L \eta' \mu_B^2 \mu_0}{\hbar V_{\text{bulb}}}, \quad (\text{C3})$$

where μ_B is the Bohr magneton, V_{bulb} is the bulb volume, and η' is the filling factor equal to

$$\eta' = \frac{V_{\text{bulb}} \langle H_z(r) \rangle_{\text{bulb}}^2}{V_c \langle H^2(r) \rangle_c}. \quad (\text{C4})$$

The classical magnetization is coupled to the rf field through Maxwell's equations. In a cavity, the relation is [21]

$$\begin{aligned} \dot{\mathbf{H}}(r, t) + (\omega_c / Q_L) \dot{\mathbf{H}}(r, t) + \omega_c^2 \mathbf{H}(r, t) \\ = \mathbf{H}_c(r) \int_{V_c} \mathbf{H}_c(r) \bullet \dot{\mathbf{M}}(r, t) dv, \end{aligned} \quad (\text{C5})$$

where ω_c is the cavity angular resonance frequency, $H_c(r)$ is the orthonormal cavity field mode, and $M(r, t)$ is the oscillating magnetization created by the coherence in the ensemble. It is given by

$$\langle M_z \rangle = \text{Tr}(\rho M_{\text{op}}). \quad (\text{C6})$$

Here M_{op} is the equivalent quantum-mechanical operator of the classical magnetization. The result is

$$\langle M_z \rangle dv = -\frac{1}{2} n \mu_B (\rho_{\mu'\mu} + \rho_{\mu\mu'}) dv, \quad (\text{C7})$$

where n is the Rb density. We write H and M in complex form:

$$\mathbf{H}(r, t) = (H^{+*}(r)e^{-i\omega t} + H^+(r)e^{i\omega t})\mathbf{z}, \quad (\text{C8})$$

$$\mathbf{M}(r, t) = (M^{+*}(r)e^{-i\omega t} + M^+(r)e^{i\omega t})\mathbf{z}, \quad (\text{C9})$$

where H^+ and M^+ are complex amplitudes of the field and of the magnetization, respectively. We replace these expressions in Eq. (C5) and, keeping only the resonant component as in the rotating wave approximation used before, we obtain

$$\begin{aligned} |\mathbf{H}| e^{-i\phi} = \frac{-iQ_L}{1 + 2iQ_L \left(\frac{\Delta\omega_c}{\omega} \right)} \mathbf{H}_c(r) \\ \times \int_{V_c} \mathbf{H}_c(r) \bullet (1/2)n\mu_B (\delta_{24}^r + i\delta_{24}^i) \mathbf{z} dv, \end{aligned} \quad (\text{C10})$$

where the off-diagonal density-matrix element has been written explicitly in complex form. Simple algebraic manipulations show that the phase of the field is given by

$$\phi = \frac{\pi}{2} + \tan^{-1} 2Q_L \frac{\Delta\omega_c}{\omega} - \tan^{-1} \frac{\delta_{24}^i}{\delta_{24}^r}, \quad (\text{C11})$$

making explicit the phase quadrature, close to $\pi/2$, between the field and the magnetization.

On the other hand, the power given by the atoms can also be obtained from Eq. (C1) by realizing that the value of H can be written in terms of the magnetization by means of Eq. (C10). One obtains

$$P_{\text{at}} = \frac{1}{2} \frac{N\hbar\omega k}{(1 + 4Q_L^2 (\Delta\omega_c / \omega_{\mu'\mu})^2)} |2\delta_{\mu'\mu}|^2. \quad (\text{C12})$$

The energy given by the ensemble compensates for the losses in the cavity. Equating Eqs. (C2) and (C12) and assuming that $2Q_L (\Delta\omega_c / \omega)$ is much smaller than 1, one obtains an interesting relation between the absolute value of the coherence $\delta_{\mu'\mu}$ and the Rabi angular frequency averaged over the interacting atomic ensemble:

$$\langle b \rangle = 2k |\delta_{\mu'\mu}|. \quad (\text{C13})$$

Equations (C11)–(C13) are those used in the main text.

ACKNOWLEDGEMENTS The author wishes to thank Claude Audoin for his constructive comments and encouragement during the writing of this text and Claude Cohen-Tannoudji for his input in connection with several parts of the analysis presented.

REFERENCES

- 1 T. Quinn (ed.), Fifty years of atomic timekeeping. Spec. issue *Metrologia*, 42 (2005)
- 2 M.W. Levine, R.F.C. Vessot, E.M. Mattison, G. Nystrom, T. Hoffman, E. Blomberg, in *Proceedings of the 31st Annual Frequency Control Symposium*, 525 (1977)
- 3 R.F.C. Vessot, E.M. Mattison, in *Proceedings of the 52nd IEEE International Frequency Control Symposium*, 336 (1998)
- 4 C. Vian, P. Rosenbusch, H. Marion, S. Bize, L. Cacciapuoti, S. Zhang, M. Arall, D. Chambon, I. Maksimovic, P. Laurent, G. Santarelli, A. Clairon, A. Luiten, M. Tobar, C. Salomon, *IEEE Trans. Instrum. Meas.* **54**, 833 (2005)
- 5 T.P. Heavner, S.R. Jefferts, E.A. Donly, J.H. Shyrlay, T.E. Parker, *IEEE Trans. Instrum. Meas.* **54**, 842 (2005)
- 6 S. Weyers, U. Hübner, R. Schröder, Chr. Tamm, A. Bauch, *Metrologia* **38**, 343 (2001)
- 7 K. Szymaniec, W. Chalupczak, P.B. Whibberley, S.N. Lea, D. Henderson, *Metrologia* **42**, 49 (2005)
- 8 I.I. Rabi, J.R. Zacharias, S. Millman, P. Kush, *Phys. Rev.* **53**, 318 (1938)
- 9 W. Gerlach, O. Stern, *Ann. Phys.* **74**, 673 (1924); *Ann. Phys.* **76**, 163 (1925)
- 10 A. Kastler, *J. Phys. Radium* **11**, 255 (1950)
- 11 G. Alzetta, A. Gozzini, M. Moi, G. Orriols, *Nuovo Cimento B* **36**, 5 (1976)
- 12 W.E. Bell, A.L. Bloom, *Phys. Rev. Lett.* **6**, 280 (1961)
- 13 M.O. Scully, M. Fleischhauer, *Phys. Rev. Lett.* **69**, 1360 (1992)
- 14 A. Nagel, L. Graf, A. Naumov, E. Mariotti, V. Biancalana, D. Meschede, R. Wynands, *Europhys. Lett.* **44**, 31 (1998)
- 15 S.E. Harris, *Phys. Today* **50**, 36 (1997)
- 16 A. Kasapi, M. Jain, G.Y. Yin, S.E. Harris, *Phys. Rev. Lett.* **74**, 2447 (1995)
- 17 M.O. Scully, M.S. Zubairy, *Quantum Optics* (Cambridge University Press, Cambridge, UK, 1999)
- 18 A. Aspect, E. Arimondo, R. Kaizer, N. Vansteenkiste, C. Cohen-Tannoudji, *J. Opt. Soc. Am. B* **6**, 2112 (1989)
- 19 R. Wynands, A. Nagel, *Appl. Phys. B* **68**, 1 (1999)
- 20 G. Avila, V. Giordano, V. Candelier, E. de Clercq, G. Théobald, P. Cérez, *Phys. Rev. A* **36**, 3719 (1987)
- 21 J. Vanier, C. Audoin, *The Quantum Physics of Atomic Frequency Standards* (Adam Hilger, Bristol, UK, 1989)
- 22 J.E. Thomas, P.R. Hemmer, S. Ezekiel, C.C. Leiby, H. Picard, R. Willis, *Phys. Rev. Lett.* **48**, 867 (1982)
- 23 N.F. Ramsey, *Phys. Rev.* **78**, 695 (1950)

- 24 N. Cyr, M. Têtu, M. Breton, *IEEE Trans. Instrum. Meas.* **42**, 640 (1993)
- 25 F. Levi, A. Godone, C. Novero, J. Vanier, in *Proceedings of the 11th European Frequency and Time Forum*, 216 (1997)
- 26 J. Vanier, A. Godone, F. Levi, *Phys. Rev. A* **58**, 2345 (1998)
- 27 J. Vanier, M. Levine, S. Kendig, D. Janssen, C. Everson, M. Delaney, in *Proceedings of the IEEE International Ultrasonics, Ferroelectrics, and Frequency Control Joint 50th Anniversary Conference*, 92 (2004)
- 28 J. Vanier, M. Levine, S. Kendig, D. Janssen, C. Everson, M. Delaney, *IEEE Trans. Instrum. Meas.* Feb. (2006)
- 29 A. Godone, F. Levi, J. Vanier, *Phys. Rev. A* **59**, R12 (1999)
- 30 F. Levi, C. Calosso, S. Micalizio, A. Godone, E.K. Bertacco, in *Proceedings of the 34th Precise Time and Time Interval (PTTI) Systems and Applications Meeting*, 139 (2002)
- 31 M. Delaney, Kernco, Inc., private communication
- 32 T. Zanon, S. Guérandel, E. De Clercq, N. Dimarcq, A. Clairon, in *Proceedings of the Joint IEEE Frequency Control Symposium/17th European Frequency and Time Forum*, 49 (2004)
- 33 R. Lutwak, D. Emmons, T. English, W. Riley, A. Duwel, M. Varghese, D.K. Serkland, G.M. Peake, in *Proceedings of the 35th Precise Time and Time Interval (PTTI) Systems and Applications Meeting*, 1 (2003)
- 34 M. Zhu, L.S. Cutler, J.E. Berberian, J.F. Denatale, P.A. Stupar, C. Tsai, in *Proceedings of the IEEE International Ultrasonics, Ferroelectrics, and Frequency Control Joint 50th Anniversary Conference*, Montréal, 100 (2004)
- 35 S. Knappe, L.-A. Liew, P. Swchwind, V. Shah, J. Moreland, L. Hollberg, J. Kitching, in *Proceedings of the IEEE International Ultrasonics, Ferroelectrics, and Frequency Control Joint 50th Anniversary Conference*, Montréal, 87 (2004)
- 36 L.-A. Liew, S. Knappe, J. Moreland, H. Robinson, L. Hollberg, J. Kitching, *Appl. Phys. Lett.* **84**, 2694 (2004); S. Knappe, P.D.D. Swchwind, V. Shah, L. Hollberg, J. Kitching, L.-A. Liew, J. Moreland, *Opt. Express* **13**, 1249 (2005)
- 37 G. Orriols, *Nuovo Cimento* **53**, 1 (1979)
- 38 A. Godone, F. Levi, S. Micalizio, J. Vanier, *Eur. Phys. J. D* **18**, 5 (2002)
- 39 J. Vanier, M. Levine, D. Janssen, M. Delaney, *Phys. Rev. A* **67**, 06581 (2003)
- 40 F. Renzoni, A. Lindner, E. Arimondo, *Phys. Rev. A* **60**, 450 (1999)
- 41 Y. Sortais, Thèse de Doctorat, Université de Paris VI, Paris, France (2001)
- 42 Y. Sortais, S. Bize, M. Abgrall, S. Zhang, C. Nicolas, C. Mandache, P. Lemonde, P. Laurent, G. Santarelli, N. Dimarcq, P. Petit, A. Clairon, A. Mann, A. Luiten, S. Chang, C. Salomon, *Phys. Scr. T* **95**, 50 (2001)
- 43 D.J. Berkeland, J.D. Miller, J.C. Bergquist, W.N. Itano, D.J. Wineland, *Phys. Rev. Lett.* **80**, 2089 (1998)
- 44 C.D. Wallace, T.P. Dinneen, K.-Y.N. Tan, T.T. Grove, P.L. Gould, *Phys. Rev. Lett.* **69**, 897 (1992)
- 45 J. Vanier, A. Godone, F. Levi, S. Micalizio, in *Proceedings of the IEEE International Frequency Control Symposium & PDA Exhibition Jointly with the 17th European Frequency and Time Forum*, 2 (2003)
- 46 E. Arimondo, in *Progress in Optics*, ed. by E. Wolf (Elsevier, Amsterdam), 257 (1996)
- 47 F. Levi, A. Godone, S. Micalizio, J. Vanier, in *Proceedings of the 31st Precise Time and Time Interval (PTTI) Systems and Applications Planning Meeting*, 216 (1999)
- 48 R.H. Dicke, *Phys. Rev. Lett.* **18**, 472 (1953)
- 49 P.R. Hemmer, S. Ezekiel, C.C. Leiby, Jr., *Opt. Lett.* **8**, 440 (1983)
- 50 P.R. Hemmer, G.P. Ontai, A. Rosenberg, S. Ezekiel, in *Proceedings of the 39th Annual Frequency Control Symposium*, 88 (1985)
- 51 P.R. Hemmer, G.P. Ontai, S. Ezekiel, *J. Opt. Soc. Am. B* **3**, 219 (1986)
- 52 M.S. Shahriar, P.R. Hemmer, *Phys. Rev. Lett.* **65**, 1865 (1990)
- 53 P.R. Hemmer, M.S. Shahriar, V.D. Natoli, S. Ezekiel, *J. Opt. Soc. Am. B* **6**, 1519 (1989)
- 54 P.R. Hemmer, M.S. Shahriar, H. Lamela-Rivera, S.P. Smith, B.E. Bernacki, S. Ezekiel, *J. Opt. Soc. Am. B* **10**, 1326 (1993)
- 55 J.H. Kim, D. Cho, *J. Korean Phys. Soc.* **37**, 744 (2000)
- 56 A.G. Mungall, *Phys. Rev. Lett.* **50**, 548 (1983)
- 57 J. Vanier, M. Levine, D. Janssen, M. Delaney, in *Proceedings of the 6th Symposium on Frequency Standards and Metrology*, ed. by P. Gill (World Scientific, London), 155 (2001)
- 58 J. Vanier, M. Levine, D. Janssen, M. Delaney, *IEEE Trans. Instrum. Meas.* **52**, 822 (2003)
- 59 J. Vanier, L.G. Bernier, *IEEE Trans. Instrum. Meas.* **30**, 277 (1981)
- 60 J. Vanier, in *Proceedings of the IEEE International Frequency Control Symposium & PDA Exhibition*, 424 (2002)
- 61 J. Vanier, M. Levine, D. Janssen, M. Delaney, *IEEE Trans. Instrum. Meas.* **52**, 258 (2003)
- 62 N. Sagna, C. Mandache, P. Thomann, in *Proceedings of the 6th European Frequency and Time Forum*, 521 (1992)
- 63 J.C. Camparo, W.F. Buell, in *Proceedings of the 51st IEEE International Frequency Control Symposium*, 253 (1997)
- 64 J.G. Coffey, M. Anderson, J.C. Camparo, *Phys. Rev.* **65**, 033807 (2002)
- 65 Y.Y. Jau, E. Miron, A.B. Post, N.N. Kuzma, W. Happer, *Phys. Rev. Lett.* **93**, 160 802 (2004)
- 66 A.V. Taichenachev, V.I. Yudin, V.L. Velichansky, S.V. Kargapol'tsev, R. Wynands, J. Kitching, L. Hollberg, *JETP Lett.* **80**, 23 (2004)
- 67 S.V. Kargapol'tsev, J. Kitching, L. Hollberg, A.V. Taichenachev, V.L. Velichansky, V.I. Yudin, *Laser Phys. Lett.* **1**, 495 (2004)
- 68 T. Zanon, S. Tremine, S. Guérandel, E. De Clercq, D. Holleville, N. Dimarcq, A. Clairon, *IEEE Trans. Instrum. Meas.* **54**, 776 (2005)
- 69 J. Vanier, R. Kanski, N. Cyr, M. Têtu, *J. Appl. Phys.* **53**, 5387 (1982)
- 70 J.P. Barrat, C. Cohen-Tannoudji, *J. Phys. Radium* **22**, 329 (1961)
- 71 L.L. Lewis, M. Feldman, in *Proceedings of the 35th Annual Frequency Control Symposium*, 612 (1981)
- 72 J. Vanier, F. Levi, A. Godone, in *Proceedings of the 1999 Joint Meeting of European Frequency and Time Forum and the IEEE International Frequency Control Symposium*, 96 (1999)
- 73 F. Levi, A. Godone, J. Vanier, *IEEE Trans. Ultrason. Ferroelectr. Freq. Control* **47**, 466 (2000)
- 74 M. Zhu, L. Cutler, in *Proceedings of the 32nd Precise Time and Time Interval (PTTI) Systems and Applications Meeting*, 311 (2000)
- 75 F. Levi, A. Godone, J. Vanier, S. Micalizio, G. Modugno, *Eur. Phys. J. D* **12**, 53 (2000)
- 76 A.V. Taichenachev, A.M. Tumaikin, V.I. Yudin, M. Stähler, R. Wynands, J. Kitching, L. Hollberg, *Phys. Rev. A* **69**, 024501 (2004)
- 77 A. Godone, F. Levi, S. Micalizio, *Coherent Population Trapping Maser* (CLUT Editrice, Torino, Italy, 2002)
- 78 T. Lindvall, M. Merimaa, I. Tittonen, E. Ikonen, in *Proceedings of the 6th Symposium on Frequency Standards and Metrology*, ed. by P. Gill (World Scientific, London), 183 (2001)
- 79 M. Merimaa, T. Lindvall, I. Tittonen, E. Ikonen, *J. Opt. Soc. Am. B: Opt. Phys.* **20**, 273 (2003)
- 80 J. Vanier, J.F. Simard, J.S. Boulanger, *Phys. Rev. A* **9**, 1031 (1974)
- 81 J.E. Kitching, H.G. Robinson, L. Hollberg, in *Proceedings of the 6th Symposium on Frequency Standards and Metrology*, ed. by P. Gill (World Scientific, London), 167 (2001)
- 82 J. Kitching, S. Knappe, N. Vukicevic, L. Hollberg, R. Wynands, W. Weidmann, *IEEE Trans. Instrum. Meas.* **49**, 1313 (2000)
- 83 W. Happer, private communication
- 84 A.B. Post, Y.Y. Jau, N.N. Kuzma, M.V. Romalis, W. Happer, in *Program of the 2004 IEEE International Ultrasonics, Ferroelectrics, and Frequency Control Joint 50th Anniversary Conference*, Montréal, August 2004, Abstracts booklet, p. 341 (not published)
- 85 Y.Y. Jau, A.B. Post, N.N. Kuzma, A.M. Braun, M.V. Romalis, W. Happer, in *Proceedings of the 2003 IEEE International Frequency Control Symposium & PDA Exhibition Jointly with the 17th European Frequency and Time Forum*, 33 (2003)
- 86 Y.Y. Jau, A.B. Post, N.N. Kuzma, A.M. Braun, M.V. Romalis, W. Happer, *Phys. Rev. Lett.* **92**, 110 801 (2004)
- 87 M. Zhu, in *Proceedings of the 2003 IEEE International Frequency Control Symposium & PDA Exhibition Jointly with the 17th European Frequency and Time Forum*, 16 (2003)
- 88 G. Miletì, J.Q. Deng, F.L. Walls, J.P. Lowe, R.E. Drullinger, in *Proceedings of the 50th IEEE International Frequency Control Symposium*, 1066 (1996)
- 89 G. Miletì, J.Q. Deng, F.L. Walls, D.A. Jennings, R.E. Drullinger, *IEEE J. Quantum Electron.* **34**, 233 (1998)
- 90 J. Vanier, *Phys. Rev.* **168**, 129 (1968)
- 91 J. Vanier, F. Strumia, *Can. J. Phys.* **54**, 2355 (1976)
- 92 A. Godone, F. Levi, S. Micalizio, J. Vanier, *Phys. Rev. A* **62**, 053402 (2000)
- 93 A. Godone, F. Levi, S. Micalizio, *Phys. Rev. A* **65**, 033802 (2002)
- 94 H. Gibbs, Ph.D. thesis, Lawrence Radiation Laboratory, University of California (1965)
- 95 A. Godone, F. Levi, S. Micalizio, C. Calosso, *Phys. Rev. A* **70**, 012508 (2004)
- 96 A. Godone, F. Levi, S. Micalizio, private communication
- 97 N. Dimarcq, E. Acouturier, G. Champagne, M. Tchagaspanian, in *Proceedings of the Fifth Symposium on Frequency Standards and Metrology*, ed. by J.C. Bergquist (World Scientific, London), 115 (1995)

- 98 A. Guillemot, G. Vareille, C. Valentin, N. Dimarcq, in *Proceedings of the 11th European Frequency and Time Forum*, 156 (1997)
- 99 E. Guillot, P.E. Pottie, C. Valentin, P. Petit, N. Dimarcq, HORACE. In *Proceedings of the Joint Meeting of the European Frequency and Time Forum and the IEEE International Frequency Control Symposium*, 81 (1999)
- 100 M. Arditì, T.R. Carver, *IEEE Trans. Instrum. Meas.* **13**, 146 (1964)
- 101 A. Godone, S. Micalizio, F. Levi, *Phys. Rev. A* **70**, 023409 (2004)
- 102 S. Trémine, S. Guérandel, D. Holeville, A. Clairon, N. Dimarcq, in *Proceedings of the IEEE International Frequency Control Symposium*, 65 (2004)
- 103 T. Zanon, S. Guérandel, E. De Clercq, D. Holeville, N. Dimarcq, A. Clairon, *Phys. Rev. Lett.* **94**, 193002 (2005)
- 104 F. Levi, S. Micalizio, A. Godone, C. Calosso, E.K. Bertacco, in *Proceedings of the IEEE International Frequency Control Symposium & PDA Exhibition Jointly with the 17th European Frequency and Time Forum*, 22 (2003)
- 105 M. Levine, D. Janssen, C. Everson, private communication
- 106 T. Zanon, private communication
- 107 M.S. Shahriar, P.R. Hemmer, D.P. Katz, A. Lee, M.G. Prentiss, *Phys. Rev. A* **55**, 2272 (1997)
- 108 R.E. Collin, *Field Theory of Guided Waves*, 2nd edn. (IEEE, New York, 1991)